JEM Journal of Experimental Medicine

ARTICLE

Ca^{2+}–mitochondria axis drives cell division in hematopoietic stem cells

Terumasa Umemoto[1], Michihiro Hashimoto[1], Takayoshi Matsumura[2], Ayako Nakamura-Ishizu[2], and Toshio Suda[1,2]

Most of the hematopoietic stem cells (HSCs) within the bone marrow (BM) show quiescent state with a low mitochondrial membrane potential ($\Delta\Psi_m$). In contrast, upon stress hematopoiesis, HSCs actively start to divide. However, the underlying mechanism for the initiation of HSC division still remains unclear. To elucidate the mechanism underlying the transition of cell cycle state in HSCs, we analyzed the change of mitochondria in HSCs after BM suppression induced by 5-fluoruracil (5-FU). We found that HSCs initiate cell division after exhibiting enhanced $\Delta\Psi_m$ as a result of increased intracellular Ca^{2+} level. Although further activation of Ca^{2+}–mitochondria pathway led to loss of HSCs after cell division, the appropriate suppression of intracellular Ca^{2+} level by exogenous adenosine or Nifedipine, a Ca^{2+} channel blocker, prolonged cell division interval in HSCs, and simultaneously achieved both cell division and HSC maintenance. Collectively, our results indicate that the Ca^{2+}–mitochondria pathway induces HSC division critically to determine HSC cell fate.

Introduction

Hematopoietic stem cells (HSCs) play a key role in the lifelong maintenance of hematopoiesis through self-renewal and multilineage differentiation. Adult HSCs reside within a specialized microenvironment of the bone marrow (BM), called "niche," in which they are maintained in a quiescent state. Because the loss of HSC quiescence leads to the exhaustion or aging of stem cells through excess cell division, the maintenance of quiescence in HSCs is essential for hematopoietic homeostasis (Mendelson and Frenette, 2014). A feature of quiescent HSCs is their low baseline energy production; quiescent HSCs exhibit low mitochondria membrane potentials ($\Delta\Psi_m$) and rely on glycolysis (Suda et al., 2011; Ito and Suda, 2014). Likewise, HSCs with a low $\Delta\Psi_m$ show greater engraftment, compared with cells with high $\Delta\Psi_m$ (Vannini et al., 2016). These reports exhibit that the maintenance of quiescent HSCs do not rely on mitochondrial metabolism.

Upon stress hematopoiesis, HSCs are forced to exit quiescence and either self-renew or differentiate to mature hematopoietic cells. HSCs exit quiescence and actively cycle upon interferon treatment or 5-fluoruracil (5-FU)–induced BM suppression (Harrison and Lerner, 1991; Essers et al., 2009; Baldridge et al., 2010). The mechanism that determines whether HSCs self-renew or differentiate during stress hematopoiesis remains unclear. The study on the activation of HSCs has not been progressed much compared with quiescent HSCs. Indeed, in addition to the low frequency of active HSCs at steady-state, a definition or prospective marker that distinguishes between quiescent and active HSCs at steady-state has not been well established. Moreover, stress hematopoietic events change the phenotypes of HSCs in BM, thereby making the accurate identification of HSCs in numbers difficult (Pietras et al., 2014), which appears to constitute a bottleneck in the study concerning active HSCs.

The influx of Ca^{2+} into mitochondria is required for the activation of mitochondria (Hajnóczky et al., 1995; Jouaville et al., 1999). Since the up-regulation of intracellular Ca^{2+} level triggers mitochondrial Ca^{2+} level (Hajnóczky et al., 1995), the control of the former appears to play a key role in mitochondrial activity. Intracellular Ca^{2+} level is regulated by ER-mediated release/uptake of Ca^{2+}, Ca^{2+} channel–mediated influx, and the efflux by Ca^{2+} pump or Na^+/Ca^{2+} exchanger. Recently, purine receptors including P2X, P2Y and adenosine receptors were reported to be involved in the regulation of intracellular Ca^{2+} (Ralevic and Burnstock, 1998; Svenningsson et al., 1999; Jiang et al., 2017). Although P2Y14 receptor is known for regulating HSCs under stress (Cho et al., 2014), the role of Ca^{2+} level in HSC maintenance still remains largely unknown.

In this study, we elucidated the mechanism underlying the initiation of cell division in HSC during stress hematopoiesis. We mainly focus on the change of energy metabolism in HSCs after BM suppression following 5-FU administration. While quiescent HSCs show low $\Delta\Psi_m$, enhanced $\Delta\Psi_m$ as a result of increased intracellular Ca^{2+} level is required for HSC division in vivo and in vitro. Moreover, we found that extracellular adenosine negatively

[1]International Research Center for Medical Sciences, Kumamoto University, Japan; [2]Cancer Science Institute of Singapore, National University of Singapore, Singapore.

Correspondence to Terumasa Umemoto: umemoto@kumamoto-u.ac.jp; Toshio Suda: csits@nus.edu.sg.

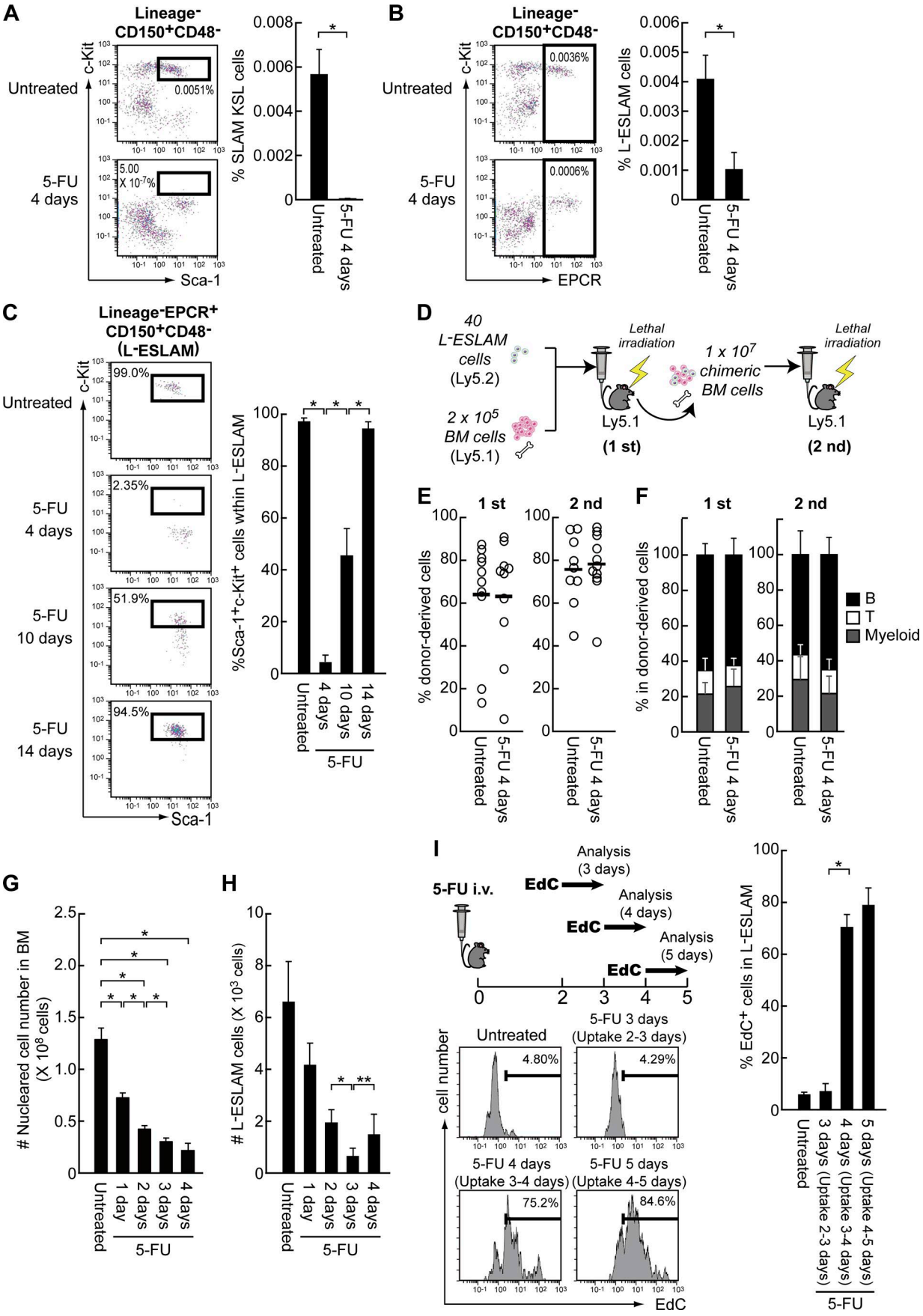
A
Lineage⁻ CD150⁺CD48⁻
Untreated
5-FU 4 days
c-Kit
Sca-1
0.0051%
5.00 X 10⁻⁷%
% SLAM KSL cells
Untreated
5-FU 4 days
B
Lineage⁻ CD150⁺CD48⁻
0.0036%
0.0006%
EPCR
% L-ESLAM cells
C
Lineage⁻EPCR⁺ CD150⁺CD48⁻ (L-ESLAM)
99.0%
2.35%
51.9%
94.5%
5-FU 10 days
5-FU 14 days
%Sca-1⁺c-Kit⁺ cells wthin L-ESLAM
4 days
10 days
14 days
5-FU
D
40 L-ESLAM cells (Ly5.2)
2 x 10⁵ BM cells (Ly5.1)
Lethal irradiation
Ly5.1
(1 st)
1 x 10⁷ chimeric BM cells
(2 nd)
E
1 st
2 nd
% donor-derived cells
F
% in donor-derived cells
B
T
Myeloid
G
Nucleared cell number in BM (X 10⁸ cells)
1 day
2 days
3 days
4 days
H
L-ESLAM cells (X 10³ cells)
I
5-FU i.v.
Analysis (3 days)
EdC
Analysis (4 days)
Analysis (5 days)
5-FU 3 days (Uptake 2-3 days)
4.80%
4.29%
5-FU 4 days (Uptake 3-4 days)
5-FU 5 days (Uptake 4-5 days)
75.2%
84.6%
cell number
EdC
% EdC⁺ cells in L-ESLAM
3 days (Uptake 2-3 days)
4 days (Uptake 3-4 days)
5 days (Uptake 4-5 days)

regulates $\Delta\Psi_m$ of HSCs after 5-FU administration. Importantly, when HSC divisions were induced, the appropriate suppression of $\Delta\Psi_m$ achieved both cell division and the maintenance of HSC functions. Our data indicate that the Ca^{2+}–mitochondria pathway plays a key role not only in initiating HSC divisions but also determining self-renewing or differentiation divisions.

Results

HSCs show enhanced $\Delta\Psi_m$ following intracellular Ca^{2+} up-regulation before entering cell cycle

To examine the mechanism underlying HSC cell cycle entry, we first focused on the change of a HSC population after BM suppression following 5-FU administration. Although $CD150^+$C-$D48^-$c-$Kit^+Sca\text{-}1^-lineage^-$ ($CD150^+CD48^-$ KSL; SLAM KSL) cells have been regarded as one of most reliable fractions for HSC identification, these cells were drastically reduced at 4 d after 5-FU administration (Fig. 1 A). All mice treated with this dose (250 mg/kg) of 5-FU could survive for >3 mo (unpublished data), and it is likely that 5-FU administration appears to alter the expression pattern of Sca-1 or c-Kit in HSCs rather than the drastic depletion of HSCs. To circumvent the change in HSC surface marker phenotype during the recovery from 5-FU–induced BM suppression, we used Endothelial protein C receptor (EPCR)-based fraction, $lineage^-EPCR^+CD150^+CD48^-$ (L^-ESLAM), for the identification of HSCs, since we and others previously found that EPCR contributes to the accurate identification of HSCs without relying on Sca-1 or c-Kit (Kent et al., 2009; Umemoto et al., 2017). L^-ESLAM population was certainly decreased by 5-FU administration, but could be stably detected (Fig. 1 B). Indeed, most of the L^-ESLAM population showed $Sca\text{-}1^+$c-Kit^+ phenotype in untreated mice, while L^-ESLAM cells in 5-FU–administrated mice were different from $Sca\text{-}1^+$c-Kit^+ gate (Fig. 1 C). However, L^-ESLAM cells started to regain $Sca\text{-}1^+$c-Kit^+ phenotype at 10 d after 5-FU administration and almost completed after 14 d (Fig. 1 C). Moreover, c-kit^{Low} L^-ESLAM cells derived from mice treated with 5-FU after 4 d showed similar engraftment and lineage contributions compared with c-kit^{High} L^-ESLAM cells obtained from untreated mice after primary and secondary transplantation (Fig. 1, C–F). These data indicate that L^-ESLAM fraction not only more accurately determines HSCs in 5-FU–treated mice rather than a fraction based on $Sca\text{-}1^+$c-Kit^+ population, but also equivalently identify stem cells both before and after 5-FU administration without any changes of gating.

We next examined the change of HSC (L^-ESLAM) number after 5-FU administration. Although BM nucleated cell number was decreased at 4 d after 5-FU treatment (Fig. 1 G), the number of L^-ESLAM HSCs recovered from day 3 and later (Fig. 1 H). Consistent with these results, uptake of EdC in L^-ESLAM cells was significantly increased from 3 d after 5-FU administration (Fig. 1 I). These data indicate that HSC division is initiated from between 3 and 4 d after 5-FU administration.

Indeed, ∼80% or >95% of L^-ESLAM cells show the uptake of EdC for 24 (Fig. 1 I) or 48 h (Fig. S1 A) from 4 d after 5-FU administration, respectively, which suggests that most of L^-ESLAM cells in mice treated with 5-FU after 4 d prospectively initiate cell division. Therefore, to examine the mechanism of HSC division initiation after 5-FU administration, "quiescent" HSCs (derived from untreated mice) and "cycling" HSCs (derived from mice treated with 5-FU after 4 d) were subjected to RNA sequencing (RNA-seq; Fig. 2 A). Consistent with the cell cycle state of HSCs, gene set enrichment analysis (GSEA) showed that gene sets related to "mitotic spindle" and "G2M check point" were enriched within up-regulated genes in cycling HSCs (Table 1 and Fig. 2 B). In addition, up-regulated genes in cycling HSCs showed significant enrichment of gene sets related to "mTOR1 signaling," "glycolysis," "reactive oxygen species," and "oxidative phosphorylation" (Table 1 and Fig. 2 B). These data suggest that the cell cycle entry of HSCs is associated with a change of energy metabolism. Since "quiescent" L^-ESLAM HSCs originally exhibited low $\Delta\Psi_m$ compared with other progenitor or mature cell fractions at steady-state (Fig. S1 B), we examined whether mitochondrial activity was changed between "cycling" and "quiescent" HSCs. To analyze the mitochondrial function of HSCs after 5-FU administration, we used red fluorescence of JC-1 (JC-1 Red), an indicator for $\Delta\Psi_m$, and found that $\Delta\Psi_m$ was significantly enhanced in "cycling" HSCs at 4 d after 5-FU administration compared to "quiescent" HSCs (Fig. 2 C). Simultaneously, "cycling" HSCs showed increased green fluorescence of JC-1 (JC-1 Green), which reflects mitochondrial mass, compared with "quiescent" HSCs (Fig. S1 C). Moreover, mitochondrial superoxide level and intracellular ATP content was also increased in "cycling" HSCs (Fig. 2, D and E). Furthermore, "cycling" HSCs appear to show increased glycolysis, as indicated by up-regulated uptake of 2-deoxy-2-[(7-nitro-2,1,3-benzoxadiazol-4-yl)amino]-D-glucose (2-NBDG), known as a fluorescent glucose analogue (Fig. S1 D). These data indicated that "cycling" HSCs derived from mice treated with 5-FU after 4 d show more activation of energy metabolism through the enhancement of mitochondrial functions along with glycolysis, compared with "quiescent" HSCs. Importantly, the time course of $\Delta\Psi_m$ up-regulation (Fig. 2 C) and EdC uptake (Fig. 1 F) indicates

Figure 1. **Cycling HSCs appear in BM after 5-FU administration. (A and B)** The frequency of SLAM KSL (A) or L^-ESLAM fraction (B) within total BM in untreated mice or 5-FU–treated mice (250 mg/kg, i.v.; $n = 4$, two independent experiments). **(C)** Expression of Sca-1/c-Kit within L^-ESLAM fraction in untreated mice or 5-FU–treated mice. Data are presented as means ± SD ($n = 4$, two independent experiments). **(D–F)** Experimental scheme for serial transplantation assay (D). After 20 wk from first or second transplantation, peripheral blood was analyzed. Each circle represents chimerism of donor-derived cells (% $Ly5.2^+$ cells) in peripheral blood of each recipient mice in the plot, and bars indicate mean values ($n > 9$, two independent experiments; E). Graphs depict the frequency of each linage cells within donor-derived cells in the peripheral blood of recipient mice (F). Data are presented as means ± SD ($n > 9$, two independent experiments). **(G and H)** Kinetic changes of total nucleated cell number (G) and the absolute number of L^-ESLAM HSCs (H) after 5-FU administration in BM obtained from both femurs and tibias ($n = 5$, three independent experiments). **(I)** The uptake of EdC for 24 h within L^-ESLAM HSCs after the administration of EdC administration (150 mg/kg i.p.) into 5-FU–treated mice at indicated schedule. Data are presented as means ± SD ($n = 4$, four independent experiments; *, $P < 0.01$; **, $P < 0.05$ by *t* test).

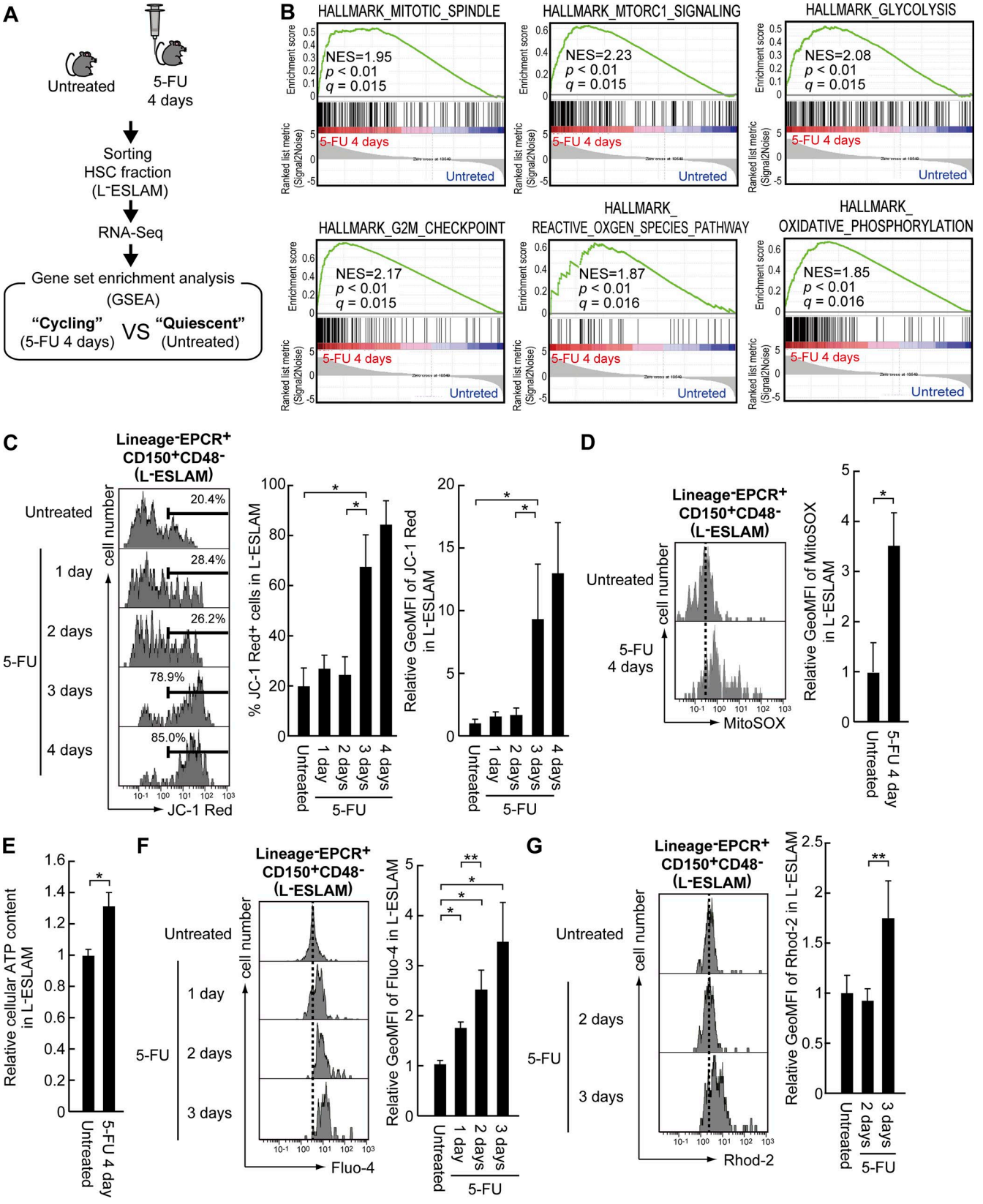

Figure 2. **HSCs show the enhancement of $\Delta\Psi_m$ following increased intracellular Ca^{2+} level immediately before entering cell cycle. (A)** GSEA following RNA-seq to compare between "cycling" HSCs derived from BM of 5-FU–treated mice (250 mg/kg, i.v. after 4 d) and "quiescent" HSCs derived from untreated mice (n = 4, two independent experiments). **(B)** Enrichment of energy metabolism–related genes within up-regulated gene in cycling HSCs. NES, normalized enrichment score; q value, false discovery rate. **(C)** Kinetic change of $\Delta\Psi_m$ in L⁻ESLAM HSCs after 5-FU treatment. Histograms show the fluorescent intensity of JC-1 Red, which reflects the height of $\Delta\Psi_m$. Graphs depict the frequency of JC-1 Red⁺ cells (left) or relative fluorescent intensity of JC-1 Red (right) in L⁻ESLAM fraction (n = 4, four independent experiments). **(D)** Mitochondrial superoxide level in L⁻ESLAM HSCs of untreated or 5-FU–treated mice (250 mg/kg, i.v.

that mitochondrial function in HSCs is enhanced immediately before the initiation of cell division.

As the influx of Ca^{2+} into mitochondria is essential for the enhancement of mitochondrial activity (Hajnóczky et al., 1995; Jouaville et al., 1999), we next examined changes in intracellular or mitochondrial Ca^{2+} level in HSCs after 5-FU administration by using Flou-4 or Rhod-2 staining, respectively (Hawkins et al., 2010; Fukumori et al., 2013; Bidaux et al., 2015). A gradual increase in intracellular Ca^{2+} level observed in HSCs after 5-FU treatment (Fig. 2 F) with significant increase in mitochondrial Ca^{2+} level at 3 d (Fig. 2 G), which coincided with enhanced $\Delta\Psi_m$ (Fig. 2 C). These data suggest that a simultaneous increase in both $\Delta\Psi_m$ and mitochondrial Ca^{2+} level following enhanced intracellular Ca^{2+} level is required for quiescent HSCs to initiate cell division.

Suppression of Ca^{2+}–mitochondria pathway leads to prolonged interval of HSC division

Next, we examined the relationship between $\Delta\Psi_m$ and intracellular Ca^{2+} level, when HSC division is induced by cytokine stimulation using the combination of stem cell factor (SCF) and thrombopoietin (TPO) in vitro. Under culture conditions that most of HSCs show more than one cell division within 48 h (5 or 50 ng/ml; Fig. 3 A), $\Delta\Psi_m$ of HSCs was significantly enhanced, which was dependent on the length of culture time (Fig. 3 B). Even culture at low concentration of cytokines (0.05 or 0.5 ng/ml) for 6 h also led to enhanced $\Delta\Psi_m$ in HSCs compared with uncultured state (Fig. 3 B). However, increase in $\Delta\Psi_m$ ceased at 18 h later (Fig. 3 B) and HSCs neither survive (0.05 ng/ml; Fig. 3 C) nor show further cell division (0.5 ng/ml) beyond this point (Fig. 3 A). Interestingly, the magnitude of $\Delta\Psi_m$ during each culture for 18 h greatly correlated to intracellular Ca^{2+} level (Fig. 3, B, D, and E) in vitro. Similarly, mitochondrial Ca^{2+} level was also increased along with intracellular Ca^{2+} level (Fig. 3 F). Although only 20% of HSCs divided at 24 h (Fig. 3 A), intracellular and mitochondrial Ca^{2+} level and $\Delta\Psi_m$ in most of HSCs already increased at 18 h of culture (Fig. 3, B, D, and F). These data support that both intracellular Ca^{2+} level and mitochondrial activity predisposed HSC division.

Next, to examine the role of Ca^{2+}–mitochondria pathway for HSC division, we treated cultured HSCs with Nifedipine, a blocker of L-type voltage-gated Ca^{2+} channels (LTCCs). Interestingly, Nifedipine significantly cancelled the increase of intracellular Ca^{2+} (Fig. 3 G) as well as mitochondrial functions including $\Delta\Psi_m$ (Fig. 3 H and Fig. S2) under conditions that induced HSC division. Similarly, Isradipine, alternative blocker of LTCCs, also suppressed both intracellular Ca^{2+} level and mitochondrial activity (Fig. S3). These data indicate that the activation of Ca^{2+}–mitochondria pathway is mainly regulated through extracellular Ca^{2+} intake. Moreover, HSC division was significantly suppressed by Nifedipine treatment (Fig. 3 I). However, CFSE dilution assay revealed that most HSCs show more than one cell division after 4 d culture even in the presence of Nifedipine, but less frequently divide in a low cytokine culture (Fig. 3 J), suggesting that Nifedipine prolonged cell division intervals.

To examine the mechanism of how Nifedipine treatment prolongs the interval of cell divisions, we tested the expression of cell cycle–related genes in HSCs cultured with or without Nifedipine. Importantly, Nifedipine treatment significantly suppressed late G1 phase–related cyclins (Cyclin E; *Ccne1* and *Ccne2*) without negatively affecting the expression of early G1 phase–related cyclins (Cyclin D; *Ccnd1*, *Ccnd2*, and *Ccnd3*; Fig. 4 A). In addition, the expression of *Cdkn1a*, also known as p21, was enhanced in Nifedipine-treated HSCs (Fig. 4 B). Consistent with these result, Nifedipine treatment decreased the phosphorylation of CDK4, CDK6, and Rb, which are known to induce Cyclin E at the late G1 phase (Fig. 4 C). These data indicate that the suppression of Ca^{2+}–mitochondria pathway during HSC division decreases the expression of Cyclin E through suppression of phosphorylation of CDK4/6-Rb axis, possibly prolonging cell division intervals.

Suppression of Ca^{2+}–mitochondria pathway prevents from loss of HSC functions during cell divisions

To examine whether Nifedipine-mediated prolonged interval of cell division affects HSC function, we analyzed the effect of cell division on HSCs using CFSE-labeling. Although HSCs cultured for 4 d under control conditions showed significant increase in CD48 expression as cell division number was increased, the addition of Nifedipine maintained a low level of CD48 expression after cell divisions (Fig. 5 A). 2-d culture with untreated controls still increased CD48 expression, even though the CFSE pattern was similar to 4-d culture with Nifedipine (Fig. 5 A). Similarly, the frequency of phenotypic HSCs within three-cell-division population was significantly decreased under control conditions (for 2 d), compared with one-cell-division population, whereas Nifedipine-treated HSCs (for 4 d) maintained ESLAM ($EPCR^+C$-$D150^+CD48^-$) KSL phenotype even after three cell divisions (Fig. 5 B). Although L^-ESLAM fraction was used to determine HSCs after 5-FU, we used ESLAM KSL fraction to carefully determine HSCs after the culture, since cultured HSCs show c-Kit^+ Sca-1^+ phenotype (Zhang and Lodish, 2005). Consistent with these results, three-cell-division population under control conditions (day 2 of culture) showed little repopulation activity upon competitive BM transplantation. In contrast, three-cell-division populations in Nifedipine treated HSCs (day 4 of culture) exhibited the engraftment in most recipients (Fig. 5 C). In addition, Nifedipine hardly affected linage contributions within recipients (Fig. 5 D). On the other hand, although low cytokine conditions similarly exhibited low intracellular Ca^{2+} level and $\Delta\Psi_m$ (Fig. 3, E and F), the maintenance of HSCs failed even after one cell division (Fig. 5 B). These results suggest that the suppression of

after 4 d). Histograms show the fluorescent intensity of MitoSOX, a mitochondrial superoxide indicator (n = 4, two independent experiments). **(E)** ATP content in L^-ESLAM HSCs in untreated or 5-FU–treated mice (250 mg/kg, i.v. after 4 d). Data are expressed as the mean ± SD (n = 4, two independent experiments). **(F and G)** Kinetic changes of intracellular (F) or mitochondrial Ca^{2+} concentration (G) in L^-ESLAM HSCs after 5-FU administration. Histograms show the fluorescent intensity of Fluo-4 (intracellular Ca^{2+} level) or Rhod-2 (mitochondrial Ca^{2+} level). Data are expressed as the mean ± SD (n = 4, two independent experiments; *, $P < 0.01$; **, $P < 0.05$ by t test).

Table 1. **Enriched gene sets within up-regulated in cycling HSCs derived from 5-FU–treated mice, as compared to quiescent HSCs derived from untreated mice**

Gene set name	Systematic name	NES	P value	Q value
HALLMARK_E2F_TARGETS	**M5925**	**1.84**	**0.042**	**0.016**
HALLMARK_NOTCH_SIGNALING	**M5913**	**1.82**	**<0.01**	**0.017**
HALLMARK_ESTROGEN_RESPONSE_LATE	**M5907**	**1.81**	**<0.01**	**0.018**
HALLMARK_MYC_TARGETS_V1	**M5926**	**1.79**	**<0.01**	**0.018**
HALLMARK_COMPLEMENT	**M5921**	**1.75**	**<0.01**	**0.02**
HALLMARK_ALLOGRAFT_REJECTION	**M5950**	**1.71**	**<0.01**	**0.021**
HALLMARK_IL2_STAT5_SIGNALING	**M5947**	**1.66**	**<0.01**	**0.022**
HALLMARK_TGF_BETA_SIGNALING	**M5896**	**1.66**	**<0.01**	**0.022**
HALLMARK_PROTEIN_SECRETION	**M5910**	**1.65**	**<0.01**	**0.022**
HALLMARK_MYC_TARGETS_V2	**M5928**	**1.65**	**<0.01**	**0.022**
HALLMARK_XENOBIOTIC_METABOLISM	**M5928**	**1.59**	**<0.01**	**0.036**
HALLMARK_APICAL_JUNCTION	M5934	1.51	0.021	0.056
HALLMARK_APOPTOSIS	M5902	1.48	0.046	0.067
HALLMARK_P53_PATHWAY	M5939	1.46	<0.01	0.073

The transcriptome data of cycling and quiescent HSCs were subjected to GSEA, and the threshold was set at P value <0.05. The normalized enrichment score (NES) reflects the degree to which a gene set is overrepresented at the top or bottom of a ranked list of genes. Bold indicates the gene sets in which q < 005.

Ca^{2+}–mitochondria pathway in the presence of cytokine stimulation contributes to the maintenance of HSCs after cell division.

In addition, gene expression analysis using RNA-Seq revealed that Nifedipine-treated ESLAM KSL HSCs within three-cell-division populations showed significantly enhanced expression of HSC markers/regulators, compared with control ESLAM KSL cells within three-division populations (Fig. 5 E). *Hoxb4, Hoxb5, Pdzk1ip1*, and *Fdg5* were well-known as markers of HSCs, and *Mecom, Spi1, Egr1, Jun, Gfi1, Foxo3, Ndn*, and *cdk1nc* contribute to the regulation of self-renewal or quiescence (Cheng et al., 2000; Zeng et al., 2004; Iwasaki et al., 2005; Miyamoto et al., 2007; Min et al., 2008; Kubota et al., 2009; Hills et al., 2011; Kataoka et al., 2011; Akada et al., 2014; Gazit et al., 2014; Chen et al., 2016; Sawai et al., 2016). Consistent with the up-regulation of *Gfi1, Foxo3, Ndn*, and *Cdkn1a*, which are downstream genes of p53 (Liu et al., 2009; Renault et al., 2011), the gene set "HALLMARK_P53_PATHWAY" was significantly enriched within up-regulated genes in Nifedipine-treated HSCs (Table 2). Moreover, transcriptome data revealed that up-regulated genes in Nifedipine-treated HSCs exhibited the enrichment of genes with the binding motif of *Foxo3* (Fig. 5 F) or FOXO3-targeted genes (Fig. 5 G). Furthermore, down-regulated genes in Gfi1-deficient LSK cells (compared with wild-type cells) was also enriched within up-regulated genes in Nifedipine-treated HSCs (Fig. 5 H). Collectively, these data suggest that the suppression of Ca^{2+}–mitochondria pathway contributes to the maintenance of HSCs during cell division, through the up-regulation of p53-related genes.

Extracellular adenosine regulates $\Delta\Psi_m$ in HSCs in vivo

So far, our data indicate that the appropriate regulation of Ca^{2+}–mitochondria pathway achieves both HSC division and the maintenance of stem cell functions in vitro. However, the mechanism of how Ca^{2+}–mitochondria pathway is regulated in cycling HSCs after 5-FU administration is still unknown. Although increased concentration of SCF and TPO enhances $\Delta\Psi_m$ of HSCs in vitro (Fig. 3 B), the in vivo levels of BM SCF and TPO are not significantly altered between untreated and 5-FU–treated mice (Fig. 6 A). These results indicate that enhanced HSC $\Delta\Psi_m$ after 5-FU administration does not depend on cytokine concentration. Therefore, we focused on a mechanism that maintains low $\Delta\Psi_m$ of steady-state HSCs without affecting their viability, because 48 h culture at 0.05 ng/ml SCF and TPO similarly led to low $\Delta\Psi_m$ of HSCs (Fig. 3 B) but was insufficient for most of HSCs to survive (Fig. 3 C).

As 5-FU treatment led to cell cycle entry of HSCs following the depletion of cycling cells, we hypothesized that the presence or absence of cycling hematopoietic cells with high $\Delta\Psi_m$ may affect HSC $\Delta\Psi_m$ in vivo. To validate this hypothesis, we examined lineage$^-$c-kit$^+$ fraction as a regulator for HSC $\Delta\Psi_m$, because these cells were drastically decreased after 5-FU administration (Fig. 6 B), even if decreased expression of c-kit in HSCs is considered (Fig. 1 C). Since myeloid progenitors (MPs; linage$^-$c-Kir$^+$Sca-1$^-$) showed higher $\Delta\Psi_m$ within lineage$^-$c-kit$^+$ fraction (Fig. 6 C), we examined the $\Delta\Psi_m$ of HSCs in co-culture with MPs (Fig. 6 D). Interestingly, the co-culture with MPs significantly decreased $\Delta\Psi_m$ of HSCs without affecting HSC viability, when compared with HSCs cultured without MPs (Fig. 6, D and E). Next, we predicted extracellularly secreted purine metabolites, adenosine as a mediator that is secreted by MPs to regulate HSC $\Delta\Psi_m$. The combination of antagonists for an adenosine receptor (SCH442416 for Adenosine A2a Receptor [ADORA2A]; PSB1115 for Adenosine A2b Receptor [ADORA2B]) completely cancelled the effect of MEPs on HSC $\Delta\Psi_m$ (Fig. 6 D). Consistent with this result, HSCs showed expression of *Adora2a* and *Adora2b*, but not *Adora1* and *Adora3* (Fig. 6 F). Moreover, the addition of adenosine suppressed the $\Delta\Psi_m$ of HSCs during the culture (Fig. 6 G) and decreased intracellular Ca^{2+} level in HSCs (Fig. 6 H). These data indicate that extracellular adenosine has a potential to suppress Ca^{2+}–mitochondria pathway through adenosine A2 receptors. Importantly, the co-culture with MPs greatly suppressed $\Delta\Psi_m$ of HSCs through adenosine A2 receptors, compared with the effect of adenosine alone (Fig. 6 F). In addition, this suppressive effect is relatively specific for MPs, as indicated by the results that the co-culture with BM CD45$^+$ cells failed the suppression of HSC $\Delta\Psi_m$ (Fig. S4). Therefore, these data suggested that 5-FU-induced ablation of cycling cells, especially MPs, which provide adenosine may enhance $\Delta\Psi_m$ of HSCs.

In addition to the ablation of MPs, extracellular adenosine level was decreased within BM after 5-FU administration (Fig. 7 A), which may also contribute to enhanced $\Delta\Psi_m$ of HSCs.

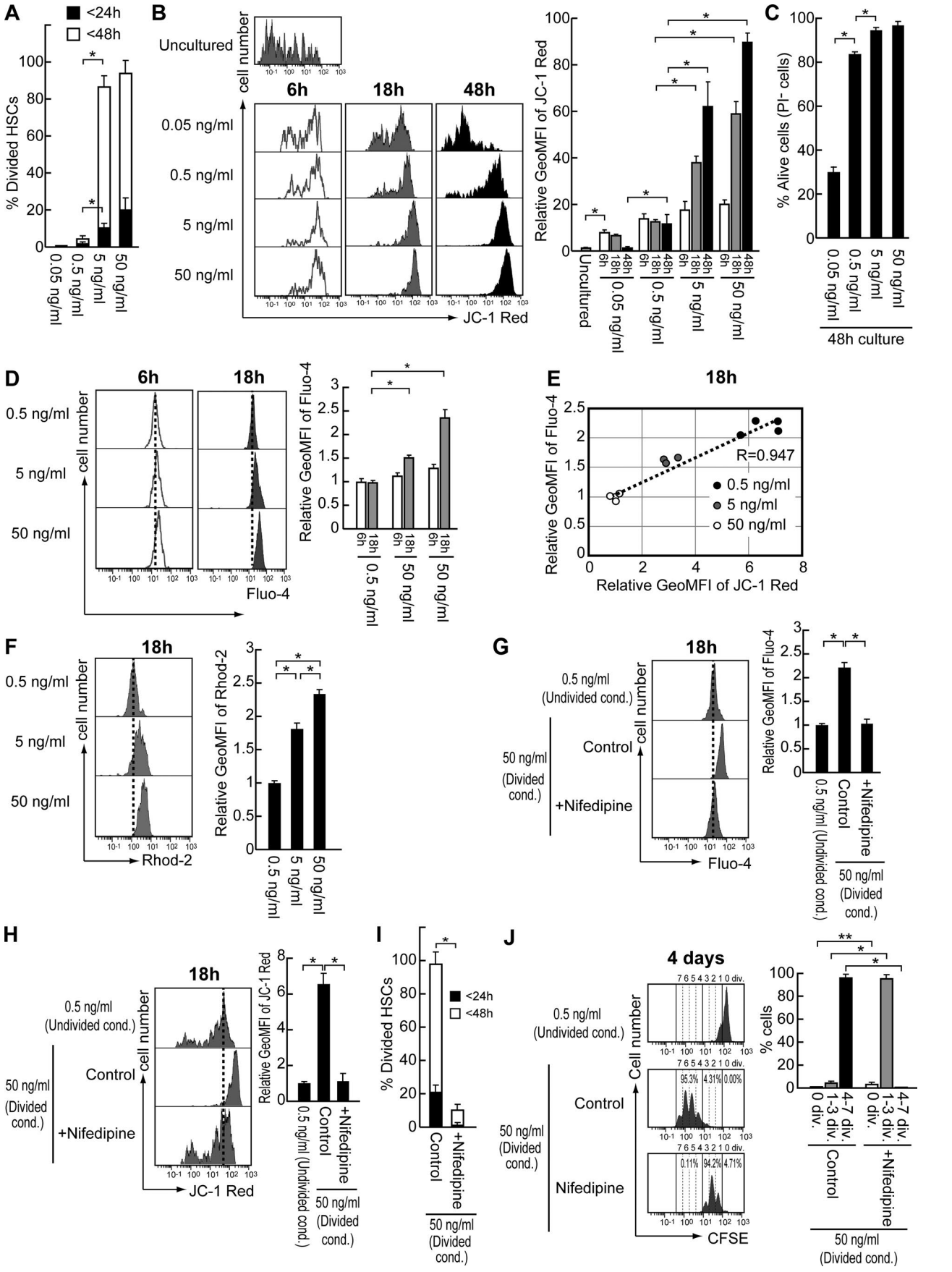
A
<24h
<48h
% Divided HSCs
0.05 ng/ml
0.5 ng/ml
5 ng/ml
50 ng/ml
B
Uncultured
cell number
6h
18h
48h
0.05 ng/ml
0.5 ng/ml
5 ng/ml
50 ng/ml
JC-1 Red
Relative GeoMFI of JC-1 Red
Uncultured
0.05 ng/ml
0.5 ng/ml
5 ng/ml
50 ng/ml
C
% Alive cells (PI- cells)
0.05 ng/ml
0.5 ng/ml
5 ng/ml
50 ng/ml
48h culture
D
6h
18h
0.5 ng/ml
5 ng/ml
50 ng/ml
cell number
Fluo-4
Relative GeoMFI of Fluo-4
0.5 ng/ml
50 ng/ml
50 ng/ml
E
18h
Relative GeoMFI of Fluo-4
R=0.947
0.5 ng/ml
5 ng/ml
50 ng/ml
Relative GeoMFI of JC-1 Red
F
18h
0.5 ng/ml
5 ng/ml
50 ng/ml
cell number
Rhod-2
Relative GeoMFI of Rhod-2
0.5 ng/ml
5 ng/ml
50 ng/ml
G
18h
0.5 ng/ml
(Undivided cond.)
50 ng/ml
(Divided
cond.)
Control
+Nifedipine
cell number
Fluo-4
Relative GeoMFI of Fluo-4
0.5 ng/ml (Undivided cond.)
Control
+Nifedipine
50 ng/ml
(Divided
cond.)
H
18h
0.5 ng/ml
(Undivided cond.)
50 ng/ml
(Divided
cond.)
Control
+Nifedipine
cell number
JC-1 Red
Relative GeoMFI of JC-1 Red
0.5 ng/ml (Undivided cond.)
Control
+Nifedipine
50 ng/ml
(Divided
cond.)
I
% Divided HSCs
<24h
<48h
Control
+Nifedipine
50 ng/ml
(Divided
cond.)
J
4 days
0.5 ng/ml
(Undivided cond.)
50 ng/ml
(Divided
cond.)
Control
Nifedipine
Cell number
7 6 5 4 3 2 1 0 div.
95.3%
4.31%
0.00%
0.11%
94.2%
4.71%
CFSE
% cells
0 div.
1-3 div.
4-7 div.
Control
+Nifedipine
50 ng/ml
(Divided cond.)

Indeed, the administration of CV1808, an agonist of Adenosine A2 receptors, after 5-FU treatment suppressed HSC both $\Delta\Psi_m$ (Fig. 7 B) and HSC division (Fig. 7 C), suggesting that decreased extracellular adenosine level triggers HSC division in 5-FU–treated mice. However, 5-FU administration only reduced 20% of baseline adenosine level. (Fig. 7 A). Furthermore, 5-FU administration did not alter the expression of *Adora2a* or *Adora2b* (Fig. 6 E). Moreover, adenosine alone could also negatively regulate their $\Delta\Psi_m$ and intracellular Ca^{2+} level (Fig. 6, F and G). Furthermore, under high cytokine conditions that induce HSC division, the treatment with CV1808 suppressed Ca^{2+}–mitochondria pathway (Fig. S5, A–E), and achieved both prolonged interval of cell division and the maintenance of low CD48 expression after cell divisions (Fig. S5 F). These data suggest that remaining adenosine alone may still affect the regulation of HSC division. To address this, we examined the effect of extracellular adenosine on HSCs in 5-FU–treated mice using antagonists for both ADORA2A and ADORA2B. Interestingly, these antagonists led to further enhance $\Delta\Psi_m$ of HSCs after 5-FU treatment (Fig. 7 D). Although ADORA2A and ADORA2B antagonists treatment did not affect BM nucleated cell number (Fig. 7 E), the frequency or number of L^-ESLAM HSC fractions were decreased (Fig. 7, F and G). Collectively, our finding exhibit that the intensity of extracellular adenosine effect not only determines HSC $\Delta\Psi_m$, but also contributes to the maintenance of HSCs after 5-FU administration (Fig. 7 H).

Discussion

The balance between quiescence and divisions in HSCs is essential for hematopoietic homeostasis. However, the mechanism of how HSCs switch from quiescence to cycling during stress hematopoiesis is unclear. Here we show that Ca^{2+}–mitochondria pathway plays a key role in the regulation of HSC division. Indeed, Ca^{2+}–mitochondria pathway was activated before HSCs started to divide in vitro and in vivo (Figs. 1–3). LTCC blockers, Nifedipine (Fig. 3, G and H; and Fig. S2) or Isradipine (Fig. S3), suppress Ca^{2+}–mitochondria pathway of HSCs and also prolong the interval of cell division through the suppression of genes that regulate late G1 phase (e.g., Cyclin E; Figs. 3 and 4). Thus, our findings indicate that the regulation of HSC cell cycle depends on the Ca^{2+}–mitochondria pathway. Moreover, the Ca^{2+}–mitochondria pathway appears to be accompanied with up-regulated potential for the uptake of glycose (Fig. S1 D). Since glycolysis is linked with mitochondrial energy metabolism, up-regulated glycolysis in HSCs may also contribute to the activation of mitochondrial functions for the initiation of cell division.

In addition to exhibiting prolonged interval of cell divisions through suppressing Ca^{2+}–mitochondria pathway, Nifedipine-treated HSCs maintained stem cell features, indicative of undifferentiated cell divisions (Fig. 5). Similarly, an agonism of adenosine A2 receptors led to both the suppression of Ca^{2+}–mitochondria pathway and slow cell divisions maintaining stem cell phenotype after HSC division (Fig. S5). In addition, $\Delta\Psi_m$ of cycling HSCs in 5-FU–treated mice was also suppressed by this agonism, which maintained HSCs (Fig. 7). In fact, GSEA showed that common gene sets such as p53, IL-2/STAT5, and Notch pathways were enriched significantly within up-regulated genes in both cycling HSCs derived from 5-FU–treated mice (Table 1) and Nifedipine-treated HSCs (Table 2). These data indicate that the effect of an agonist of adenosine A2 receptors on HSCs is recapitulated with that of LTCC blockers. Indeed, adenosine A2 receptors reportedly inhibit calcium influx via LTCCs in rod photoreceptors (Stella et al., 2002). Therefore, these data and this previous study suggest that the agonism of adenosine A2 receptors is involved in the inhibition of Ca^{2+} influx, thereby contributing to the maintenance of HSCs during continuous divisions through the suppression of Ca^{2+}–mitochondria pathway. However, it has been generally known that adenosine A2 receptors up-regulate intracellular Ca^{2+} level through the activation of Ca^{2+} channels via GαS or Gαq (Ham and Evans, 2012). However, our findings have been also supported by the recent report showing that adenosine A2a receptor contributes to the suppression of reactive oxygen species generation, a function of mitochondria (Hirata et al., 2018). Therefore, adenosine A2 receptors may negatively affect Ca^{2+}–mitochondria pathway in HSCs, probably through an unknown mechanism for the inhibition of Ca^{2+} influx.

Similar to HSCs treated with Nifedipine in high cytokine culture, HSCs cultured in a low concentration of cytokines (undivided conditions) showed suppressed Ca^{2+}–mitochondria pathway and cell division (Fig. 3). However, a low level of cytokine was insufficient for the maintenance of HSC phenotype as indicated by significant decrease in phenotypic HSCs after cell division (Fig. 5 A). Importantly, Nifedipine treatment did not negatively affect the up-regulation of early G1 phase–related genes (e.g., Cyclin D) that was induced by high cytokine concentration (Fig. 4 A). In addition, Nifedipine-treated HSCs showed enhanced expression of early response genes (e.g., *Egr1* and *Jun*), compared with HSCs cultured under control

Figure 3. **Ca^{2+} channel blocker suppresses cell division of HSCs through the down-regulation of $\Delta\Psi_m$. (A)** The frequency of divided SLAM KSL HSCs after single cell culture for 24 or 48 h (n = 4, four independent experiments). **(B and C)** $\Delta\Psi_m$ (B) or viability of HSCs (C) after the culture for 48 h under conditions as described above. Each value of $\Delta\Psi_m$ was relative to the value of uncultured HSCs (n = 5, three independent experiments). **(D and F)** Intracellular (D) or mitochondrial Ca^{2+} level (F) of HSCs cultured under indicated conditions. Data are presented as means ± SD relative to the value of cells treated with SCF and TPO at 0.5 ng/ml (undivided conditions; n > 3, two independent experiments). **(E)** The plot showing the relationship between $\Delta\Psi_m$ and intracellular Ca^{2+} level after 18 h culture under indicated conditions. R represents the correlation coefficient. **(G and H)** Intracellular Ca^{2+} level (G) or $\Delta\Psi_m$ (H) of HSCs cultured with SCF and TPO at 50 ng/ml (divided conditions) in the absence (Control) or presence of 60 µM Nifedipine (+Nifedipine). Data are presented as means ± SD relative to the value of cells treated with SCF and TPO at 0.5 ng/ml (undivided conditions; n = 4, two independent experiments). **(I and J)** The effect of Nifedipine on HSC division. Single cell culture (I) and CFSE-dilution assay (J) were performed under conditions described above. Data are presented as means ± SD (n = 4, four independent experiments; *, P < 0.01; **, P < 0.05 by t test).

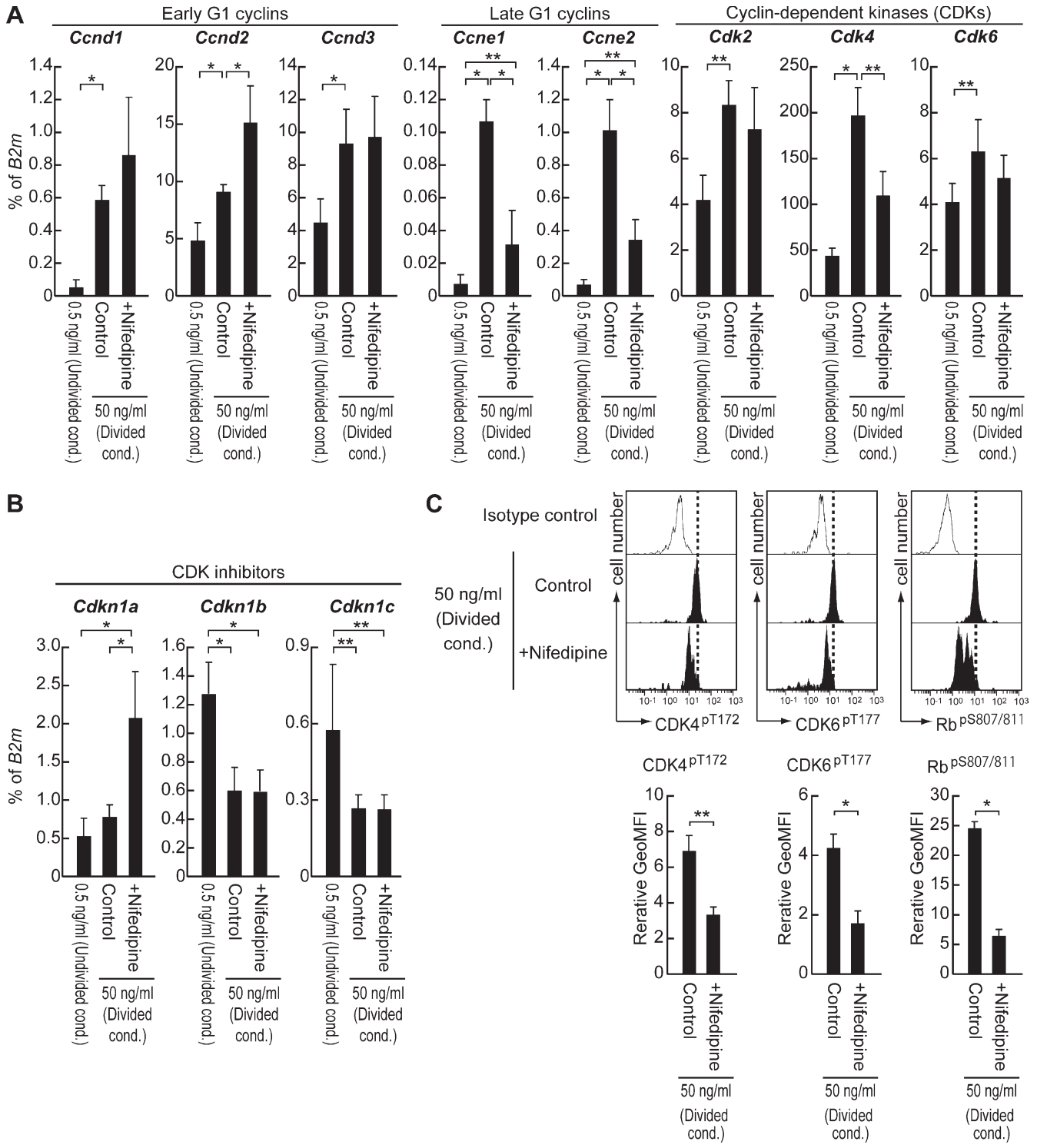

Figure 4. **Expression of cell cycle related genes is altered by the treatment with Ca^{2+} channel blocker in HSCs. (A and B)** After the culture of sorted $CD150^{+}CD48^{-}$KSL HSCs for 18 h under undivided conditions (0.5 ng/ml SCF and TPO) or divided conditions (50 ng/ml SCF and TPO) in the absence (Control) or presence of 60 µM Nifedipine (+Nifedipine), expression of Cyclins or cyclin-dependent kinase (CDKs; A) and CDK inhibitors (B) was examined by RT-PCR. Graphs depict mRNA expression level normalized by *B2m* expression (n = 6, two independent experiments). **(C)** After culturing $CD150^{+}CD48^{-}$KSL HSCs for 18 h under divided conditions (50 ng/ml SCF and TPO) in the absence (Control) or presence of 60 µM Nifedipine (+Nifedipine), phosphorylation of CDK4 at Thr172, CDK6 at Thr177 or Rb at Ser807/811 was examined by flow cytometry. Each graph depicts geometric mean fluorescence intensity (GeoMFI) relative to the value of cells stained with isotype control. Data are presented as means ± SD (n = 3, three independent experiments; *, $P < 0.01$; **, $P < 0.05$ by t test).

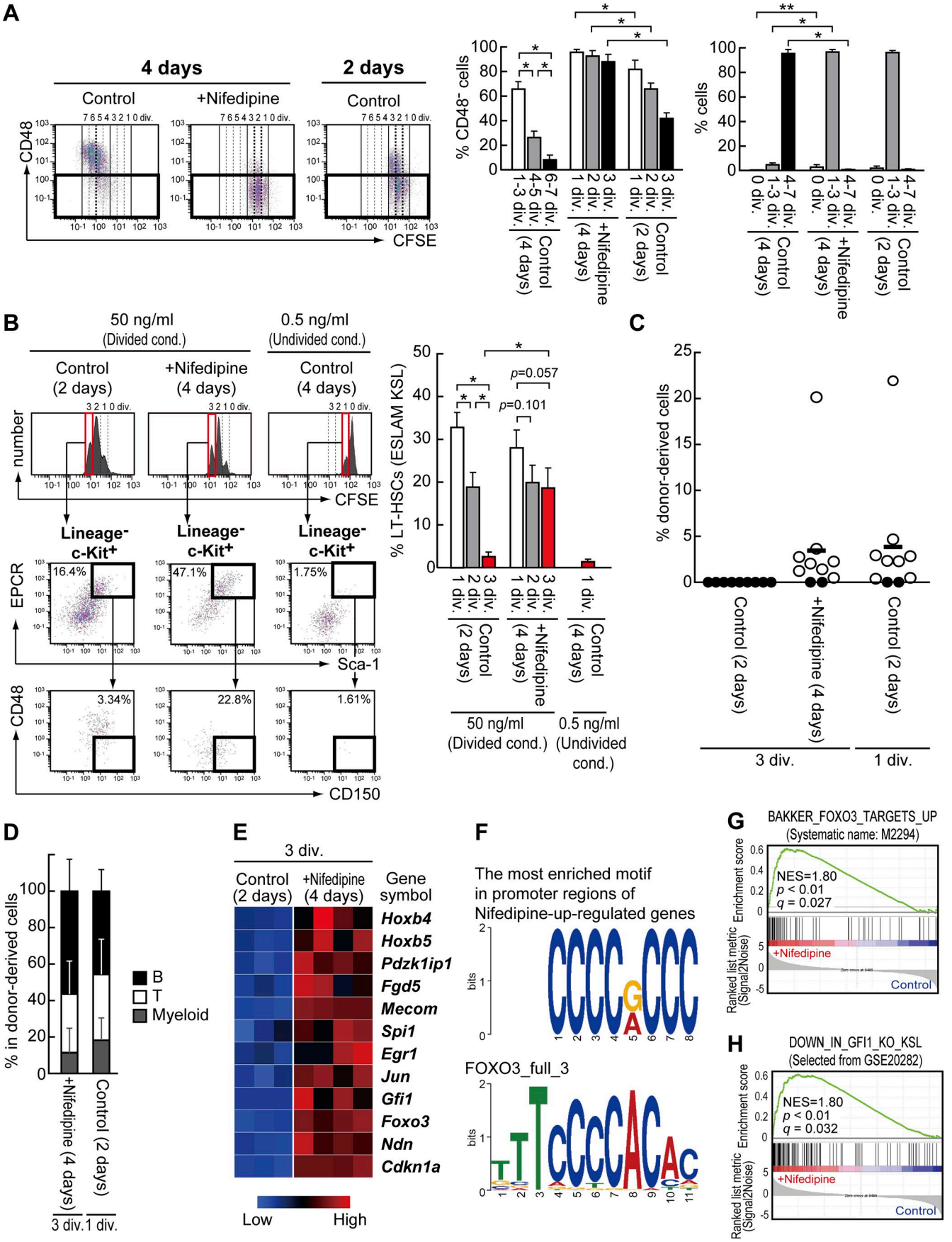
A
4 days
2 days
Control
+Nifedipine
Control
CD48
CFSE
% CD48- cells
% cells
1-3 div. (4 days) Control
4-5 div.
6-7 div.
1 div. 2 div. 3 div. (4 days) +Nifedipine
1 div. 2 div. 3 div. (2 days) Control
0 div.
4-7 div.
B
50 ng/ml (Divided cond.)
0.5 ng/ml (Undivided cond.)
Control (2 days)
+Nifedipine (4 days)
Control (4 days)
number
Lineage- c-Kit+
EPCR
Sca-1
CD150
16.4%
47.1%
1.75%
3.34%
22.8%
1.61%
% LT-HSCs (ESLAM KSL)
p=0.057
p=0.101
1 div. 2 div. 3 div. (2 days) Control
1 div. 2 div. 3 div. (4 days) +Nifedipine
1 div. (4 days) Control
50 ng/ml (Divided cond.)
0.5 ng/ml (Undivided cond.)
C
% donor-derived cells
Control (2 days)
+Nifedipine (4 days)
Control (2 days)
3 div.
1 div.
D
% in donor-derived cells
B
T
Myeloid
+Nifedipine (4 days)
Control (2 days)
3 div.
1 div.
E
3 div.
Control (2 days)
+Nifedipine (4 days)
Gene symbol
Hoxb4
Hoxb5
Pdzk1ip1
Fgd5
Mecom
Spi1
Egr1
Jun
Gfi1
Foxo3
Ndn
Cdkn1a
Low
High
F
The most enriched motif in promoter regions of Nifedipine-up-regulated genes
bits
FOXO3_full_3
G
BAKKER_FOXO3_TARGETS_UP
(Systematic name: M2294)
Enrichment score
NES=1.80
p < 0.01
q = 0.027
+Nifedipine
Control
Ranked list metric (Signal2Noise)
H
DOWN_IN_GFI1_KO_KSL
(Selected from GSE20282)
NES=1.80
p < 0.01
q = 0.032
+Nifedipine
Control

conditions (Fig. 5 E). These data suggest that the suppression of Ca^{2+}–mitochondria pathway does not disturb the reception of cytokine stimulations. Thus, the combination of Ca^{2+}–mitochondria pathway and cytokine stimulations are crucial for HSC self-renewal division.

We also demonstrated that a purine metabolite, adenosine, acts as a regulator of HSCs by suppressing the Ca^{2+}–mitochondria pathway in HSCs. (Figs. 6 and 7). Adenosine decreases $\Delta\Psi_m$ of HSCs in co-culture of HSCs with MPs without affecting their viability in vitro (Fig. 6). This suggests that MPs which are depleted with 5-FU plays a key role in HSC quiescence through providing extracellular adenosine. In addition, regulatory T cells reportedly regulates HSC quiescence through supplying extracellular adenosine (Hirata et al., 2018). Therefore, our results suggest that MPs act as a novel provider of adenosine to contribute to HSC quiescent through suppressing Ca^{2+}–mitochondria pathway. In addition to the changes in adenosine level, the ablation of surrounding hematopoietic cells after 5-FU administration may induce the dissolution of hypoxia. As non-HSC hematopoietic cells show a high $\Delta\Psi_m$, the ablation of these cells after 5-FU administration may cause a decrease in the consumption of O_2 within the BM. With that, we confirmed an increase in the number of erythrocytes within the BM after 5-FU treatment (unpublished data). In addition, hypoxia is well known as one of factors for the regulation of HSC quiescence (Takubo et al., 2010), and the dissolution of hypoxia may attenuate HSC features through alteration of $\Delta\Psi_m$ (Mantel et al., 2015). Thus, these data and this previous study support the possibility that the dissolution of hypoxia within BM after 5-FU treatment also contributes to enhanced $\Delta\Psi_m$ of HSCs.

Although both $\Delta\Psi_m$ and intracellular Ca^{2+} were simultaneously enhanced after cytokine stimulation in vitro (Fig. 3), the enhancement of $\Delta\Psi_m$ lagged behind increased intracellular Ca^{2+} level in HSCs after 5-FU administration (Fig. 2). Since the mitochondrial Ca^{2+} level was enhanced simultaneously at the same timing as $\Delta\Psi_m$ after 5-FU administration (Fig. 2), quiescent HSCs in vivo may be resistant to an influx of Ca^{2+} into mitochondria. Mitochondrial calcium uniporter (MCU) plays a key role in the influx of Ca^{2+} from cytosol to mitochondria (Kirichok et al., 2004) as well as the regulation of mitochondrial energy metabolism (Tarasov et al., 2012). Therefore, the regulation of MCU may be involved in the resistance for an influx of Ca^{2+} into mitochondria in quiescent HSCs within BM niche.

In conclusion, this study demonstrates that the activation of Ca^{2+}–mitochondria pathway precedes HSC division. The appropriate suppression of Ca^{2+}–mitochondria pathway is necessary for HSC self-renewal division. Therefore, the regulation of Ca^{2+}–mitochondria pathway is crucial for the determination of HSC cell fate (self-renewing or differentiation division). We indicate that adenosine acts as a suppressor of Ca^{2+}–mitochondria pathway to regulate HSC maintenance in vivo. Thus, our findings shed new light into understanding the mechanism for the HSC self-renewal and may also contribute to the development of ex vivo expansion of HSCs for therapeutic applications.

Materials and methods

Animals

C57BL/6-Ly5.2 and C57BL/6-Ly5.1 mice were obtained from Sankyo Labo Service Corporation or Japan SLC Inc. Each strain used was between 8 and 12 wk of age. All animal experiments were performed according to the Guidelines of Kumamoto University on Animal Use (Approval No. 29-091).

Antibodies for flow cytometry

The following monoclonal antibodies were used for cell sorting and flow cytometric analysis of surface markers: anti-c-Kit (2B8), anti-CD150 (TC15-12F12.2), anti-CD48 (HM48-1), anti-EPCR (RAM34; eBioscience), anti–Sca-1 (E13-161.7), anti-CD45.2 (104), anti-CD45.1 (A20), anti-B220/CD45R (RA3-6B2), anti–Mac-1 (M1/70), anti-Gr-1 (RB6-8C5), anti-CD4 (RM4-5), and anti-CD8 (53-6.72) antibodies. All antibodies were obtained from BioLegend unless otherwise noted.

Cell preparation

Suspensions of BM cells were prepared from mice as described previously (Umemoto et al., 2006, 2012).

5-FU administration

To induce BM suppression, mice were intravenously injected with 250 mg/kg 5-FU (Kyowa Hakko Kirin). At indicated time after the last administration, BM cells were removed for several analyses. Total nucleated cell numbers were quantified

Figure 5. **Ca^{2+} channel blocker maintains functional HSCs through up-regulating expression of HSC regulators. (A and B)** HSC phenotypes after HSC divisions in the absence (Control) or presence of 60 µM Nifedipine (+Nifedipine) for 4 or 2 d. Graphs depict the frequency of $CD48^-$ cells (A; left), cell division number (A; right) or the frequency of ESLAM LSK cells (B). The percentage in each dot plot represent the frequency of indicated fractions within one cell–division or three cell–division populations (B). Data are presented as means ± SD (n = 4, four independent experiments). **(C and D)** Transplantation assay using 50 cells derived from three-divided populations (Ly5.1) after the culture as described above, along with 2×10^5 competitor cells (Ly5.2). Open or closed circles represent donor cell chimerism in multilineage-reconstructed recipient mice or unreconstructed mice after 20 wk in the plot, respectively (C). Bars indicate mean values (n > 9, two independent experiments). The graph depicts the frequency of each linage cells within donor-derived cells (D). Data are presented as means ± SD (n = 8, two independent experiments). **(E–H)** Gene expression analyses of three-divided ESLAM LSK HSCs after the culture as described above. RNA-Seq (heat map) revealed expression level of indicated genes (n > 3, two independent experiments, P < 0.01 EdgeR, q < 0.05 by FDR; E). The most enriched motif in the promoters of genes up-regulated by nifedipine (F; upper, E value = 2.2×10^{-84}) which significantly resembles the FOXO3 binding motif (F; lower, q = 0.0492). Enrichment of Foxo3-targeted gene set "BAKKER_FOXO3_TARGETS_UP" (G) or Gfi1-dependent gene set "DOWN_IN_GFI1_KO_KSL" (H) within Nifedipine-up-regulated genes.

Table 2. **Enriched gene sets within up-regulated in Nifedipine-treated HSCs, as compared to HSCs cultured under control conditions**

Gene set name	Systematic name	NES	P value	Q value
HALLMARK_P53_PATHWAY	**M5939**	**2.00**	**<0.01**	**0.019**
HALLMARK_INFLAMMATORY_RESPONSE	**M5932**	**1.98**	**<0.01**	**0.019**
HALLMARK_APOPTOSIS	**M5902**	**1.90**	**<0.01**	**0.027**
HALLMARK_HYPOXIA	**M5891**	**1.86**	**<0.01**	**0.025**
HALLMARK_IL2_STAT5_SIGNALING	**M5947**	**1.83**	**<0.01**	**0.028**
HALLMARK_KRAS_SIGNALING_UP	**M5953**	**1.82**	**<0.01**	**0.026**
HALLMARK_UV_RESPONSE_DN	**M5942**	**1.80**	**<0.01**	**0.025**
HALLMARK_INTERFERON_ALPHA_RESPONSE	**M5911**	**1.78**	**<0.01**	**0.025**
HALLMARK_INTERFERON_GAMMA_RESPONSE	**M5913**	**1.76**	**<0.01**	**0.024**
HALLMARK_NOTCH_SIGNALING	**M5903**	**1.72**	**<0.01**	**0.029**
HALLMARK_IL6_JAK_STAT3_SIGNALING	**M5897**	**1.72**	**<0.01**	**0.028**
HALLMARK_MYOGENESIS	**M5909**	**1.58**	**<0.01**	**0.044**
HALLMARK_HEME_METABOLISM	M5945	1.55	<0.01	0.054
HALLMARK_TNFA_SIGNALING_VIA_NFKB	M5890	1.54	<0.01	0.053
HALLMARK_EPITHELIAL_MESENCHYMAL_TRANSITION	M5930	1.51	<0.01	0.062
HALLMARK_APICAL_SURFACE	M5916	1.40	0.042	0.098
HALLMARK_ESTROGEN_RESPONSE_LATE	M5907	1.38	0.05	0.106

The transcriptome data of three-cell-divided HSCs cultured with or without Nifedipine were subjected to GSEA, and the threshold was set at P value < 0.05. The normalized enrichment score (NES) reflects the degree to which a gene set is overrepresented at the top or bottom of a ranked list of genes. Bold indicates the gene sets in which q < 0.05.

using TC20 Automated Cell Counter (Bio-Rad Laboratories) after Turk staining.

Cell sorting and flow cytometric analysis

We used either FACS Aria III (BD Biosciences) or FACS CANTO II (BD Biosciences) for cell sorting and flow cytometric analyses, as described previously (Umemoto et al., 2006, 2012).

Long-term competitive repopulation assays

Long-term competitive repopulation assays were performed by transplanting the indicated cells derived from C57BL/6-Ly5.1 congenic mice into lethally irradiated (10 Gy) C57BL/6-Ly5.2 mice through i.v., as described previously (Umemoto et al., 2012). 20 wk after transplantation, recipient mice with donor cell chimerism (>0.1% for myeloid and B- and T-lymphoid lineages) were considered to be multilineage-reconstituted mice (positive mice). For serial transplantation, 10^7 whole BM cells were obtained from primary transplanted mice and transplanted into secondary irradiated recipient mice.

EdU uptake assay

Following 5-FU treatment, 150 mg/kg EdC (Tokyo Chemical Industry Co.) was i.p. administrated at an indicated point. After 24 or 48 h, cells that uptake EdC were determined by Click-iT Plus EdU Alexa Fluor 488 Flow Cytometry Assay kit (Thermo Fisher Scientific), according to the manufacturer's instruction.

RNA-seq

We performed RNA-seq as previously reported (Hayashi et al., 2018) with minor modification. In brief, using 100 sorted cells, the first strand of cDNA was synthesized by using PrimeScript RT reagent kit (TAKARA Bio Inc.) and not-so random primers. Following the synthesis of the first strand, the second strand was synthesized by using Klenow Fragment (3′-5′ exo-; New England Biolabs Inc.) and complement chains of not-so random primers. Using purified double-strand cDNA, the library for RNA-Seq was prepared and amplified using Nextera XT DNA sample Prep kit (Illumina Inc.). This prepared library was sequenced on Next-Seq system (Illumina Inc.), according to the manufacturer's instruction. In addition, each obtained read was mapped to the reference sequence "GRCm38/mm10" using CLC genomic workbench v11.0.0 (Qiagen), and expression levels were normalized and subjected to the statistical analyses based on EdgeR. All RNA-seq data were deposited in the Gene Expression Omnibus (GEO) under accession no. GSE111118. Transcriptome data were subjected to GSEA using GSEA v3.0.0 software, available from the Broad Institute (Subramanian et al., 2005). All Gene sets were obtained from the database of Broad Institute unless otherwise stated. Gfi1-dependent gene set "DOWN_IN_GFI1_KO_KSL" was extracted by a threshold setting at more than twofold changed and $P < 0.05$, after gene expression pattern between Wt and Gfi1 KO LSK cells in GEO under accession no. GSE20282 were compared.

Measurement of $\Delta\Psi_m$, intracellular Ca^{2+}, mitochondrial Ca^{2+} and mitochondrial superoxide level

The $\Delta\Psi_m$, intracellular Ca^{2+}, mitochondrial Ca^{2+}, and or mitochondrial superoxide level of indicated cells were determined according to the manufacturer's instruction using MitoProbe JC-1 Assay kit (Thermo Fisher Scientific), Fluo-4, AM (Thermo Fisher Scientific), Rhod-2, AM (Thermo Fisher Scientific), or MitoSOX Red Mitochondrial Superoxide Indicator (Thermo Fisher Scientific), respectively. In brief, cells were stained with 2 µM JC-1, 1 µM Fluo-4, AM, 1 µM Rhod-2, AM, or 5 µM MitoSOX Red for 30 min. After staining, each fluorescent intensity was determined using a flow cytometer.

The measurement of ATP content

Four hundred sorted HSCs were suspended using 25 µl S-clone SF-03 medium supplemented with 0.5% bovine serum albumin, and subsequently equivalent volume of "Cellno" ATP ASSAY reagent (TOYO B-Net Co.) was added. After 10 min, the intensity of luminescence in each sample was measured by Multi-mode Plate reader Synergy H1 (BioTek Instruments).

The measurement of glucose uptake

After total BM cells were stained by APC-conjugated anti-EPCR antibody, magnetic beads–conjugated anti-APC antibody

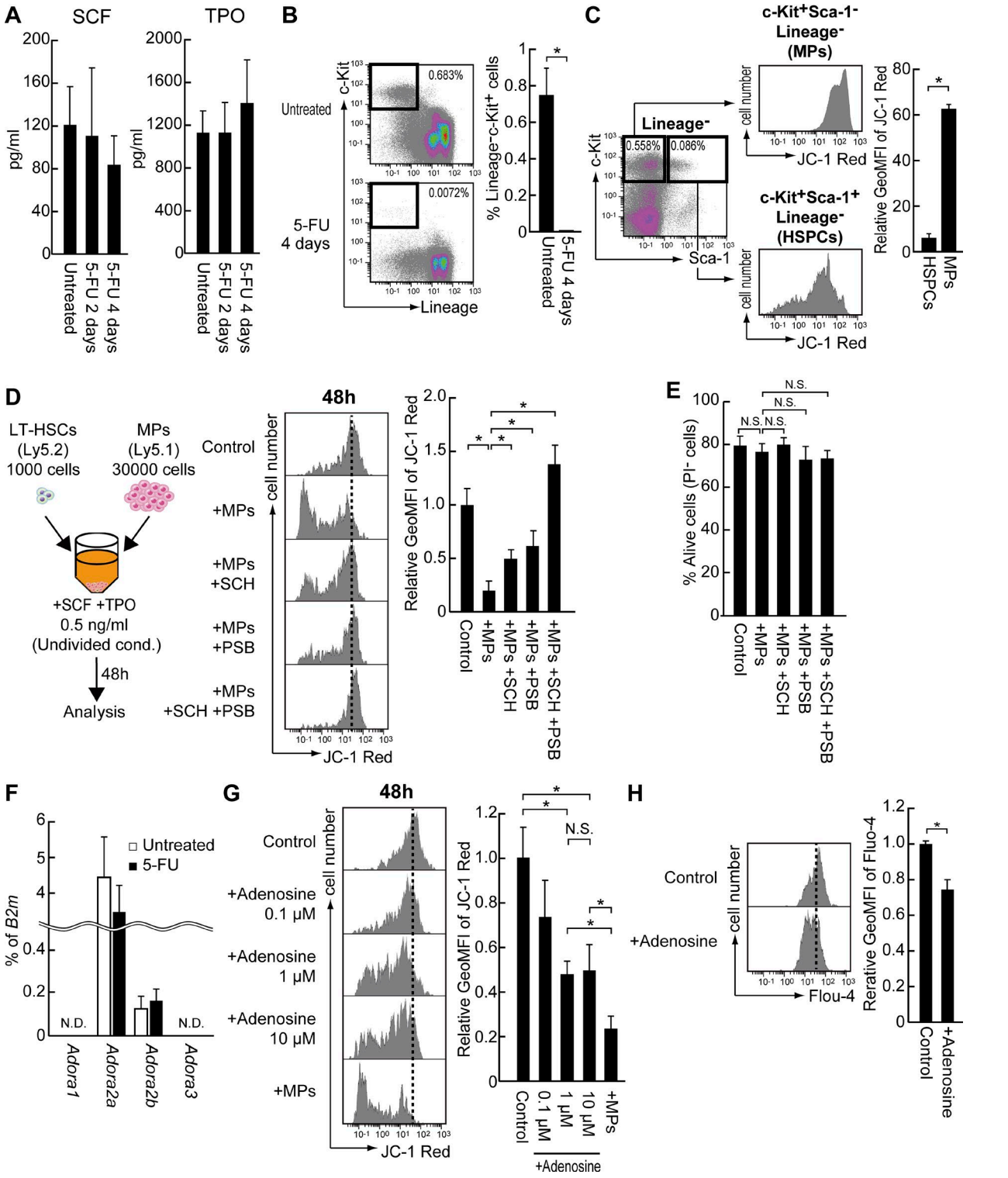

Figure 6. **Extracellular adenosine acts as a regulator to regulate Ca^{2+}–mitochondria pathway. (A)** The amount of SCF or TPO within BM in untreated or 5-FU–treated mice. Data are expressed as the mean ± SD (n = 4, two independent experiments). **(B)** The frequency of lineage⁻c-kit⁺ cells within total BM cells after 5-FU treatment (250 mg/kg, i.v; n = 4, two independent experiments). **(C)** $\Delta\Psi_m$ of indicated fractions in untreated mice. Numbers in dot plots represent the frequency of gated cells within total BM cells. Data are presented as means ± SD relative to the value of L⁻ESLAM HSCs. (n = 4, two independent experiments). **(D and E)** $\Delta\Psi_m$ (D) or viability (E) of HSCs after the co-culture of MPs (linage⁻c-Kir⁺Sca-1⁻) for 48 h in the absence or presence of 10 μM SCH442416 (SCH: Adora2a antagonist) and/or 10 μM PSB1115 (PSB: Adora2b antagonist). Cells cultured without both MPs and antagonists serve as control. n = 4, four independent experiments. **(F)** Expression of adenosine receptors in HSCs before and after 5-FU administration. Data are expressed as the mean ± SD relative to *B2m* expression (n = 4, two independent experiments by t test). **(G and H)** $\Delta\Psi_m$ (G) or intracellular Ca^{2+} level (H) in HSCs after the culture with adenosine for 48 h or immediately after the stimulation (10 μM adenosine), respectively. Cells cultured without adenosine serve as control. Data are presented as means ± SD (n = 5, three independent experiments, *, P < 0.01 by t test [G]; n = 4, two independent experiments, *, P < 0.01 by t test [H]). N.S., not significant.

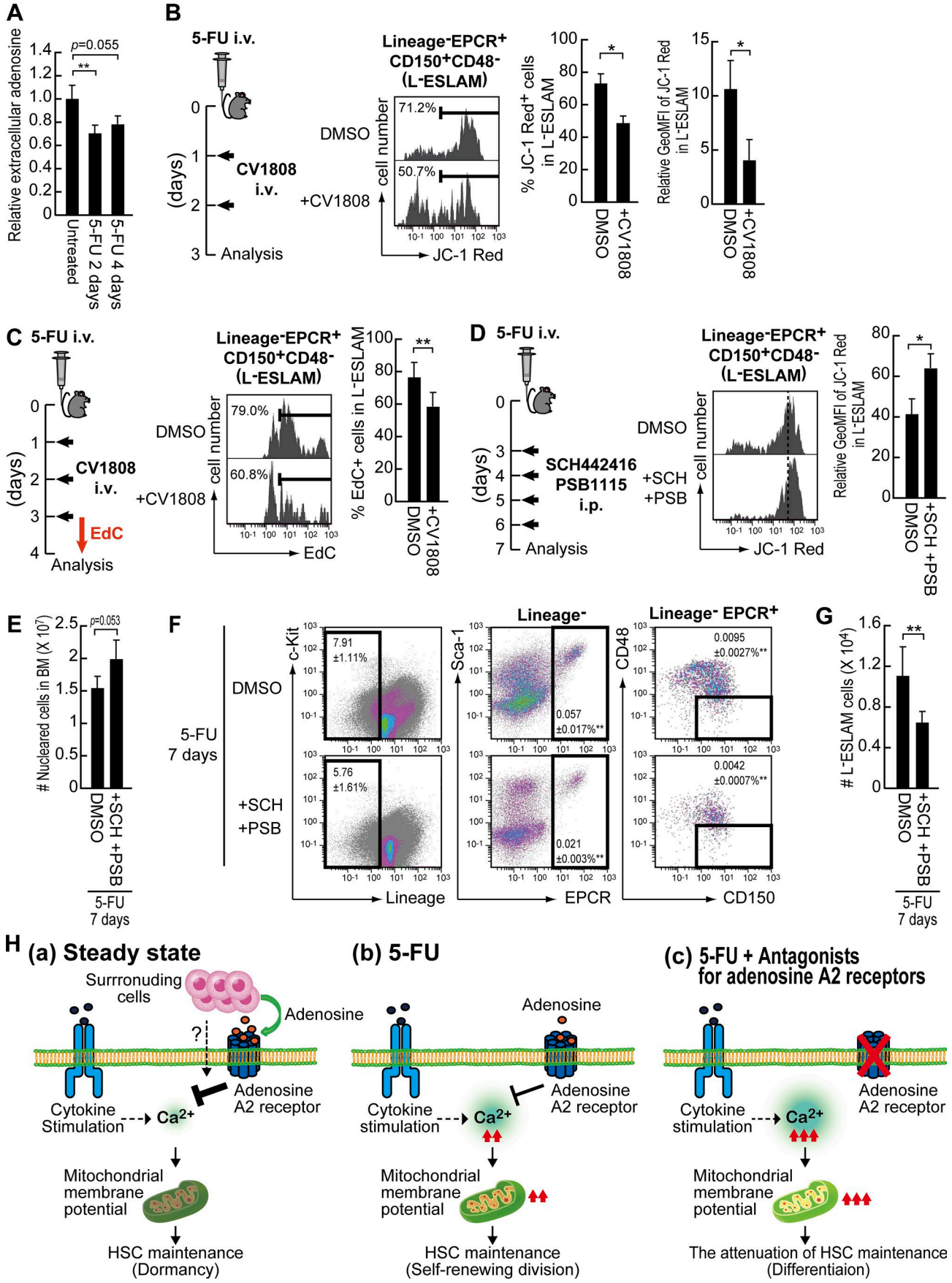
A
Relative extracellular adenosine
p=0.055
**
Untreated
5-FU 2 days
5-FU 4 days
B
5-FU i.v.
CV1808 i.v.
(days)
Analysis
Lineage-EPCR+ CD150+CD48- (L-ESLAM)
DMSO
+CV1808
71.2%
50.7%
cell number
JC-1 Red
% JC-1 Red+ cells in L-ESLAM
Relative GeoMFI of JC-1 Red in L-ESLAM
C
5-FU i.v.
CV1808 i.v.
EdC
Analysis
79.0%
60.8%
EdC
% EdC+ cells in L-ESLAM
D
5-FU i.v.
SCH442416
PSB1115
i.p.
Analysis
+SCH +PSB
E
# Nucleared cells in BM (X 10^7)
p=0.053
5-FU 7 days
F
DMSO
+SCH +PSB
5-FU 7 days
c-Kit
Sca-1
CD48
Lineage-
Lineage- EPCR+
7.91 ±1.11%
5.76 ±1.61%
0.057 ±0.017%**
0.021 ±0.003%**
0.0095 ±0.0027%**
0.0042 ±0.0007%**
Lineage
EPCR
CD150
G
L-ESLAM cells (X 10^4)
H
(a) Steady state
Surrronuding cells
Adenosine
?
Adenosine A2 receptor
Cytokine Stimulation
Ca2+
Mitochondrial membrane potential
HSC maintenance (Dormancy)
(b) 5-FU
Cytokine stimulation
HSC maintenance (Self-renewing division)
(c) 5-FU + Antagonists for adenosine A2 receptors
The attenuation of HSC maintenance (Differentiaion)

(Miltenyi Biotec) was used as secondary antibody for cell sorting by AutoMACS pro (Miltenyi Biotec). Obtained EPCR$^+$ cells were cultured with 2-NBDG using 2-NBDG Glucose Uptake Assay kit according to the manufacturer's instruction (BioVision), before staining for the identification of L$^-$ESLAM cells. The potential for glucose uptake in L$^-$ESLAM cells was determined based on the fluorescence intensity of 2-NBDG by a flow cytometer.

HSC cultures

As described previously (Umemoto et al., 2012, 2017), CD150$^+$CD48$^-$KSL HSCs were sorted and cultured for 5 d in S-Clone SF-03 medium (Sanko-Junyaku Co.) supplemented with 0.5% bovine serum albumin (Sigma), 0.05∼50 ng/ml mouse SCF and 0.05∼50 ng/ml mouse TPO (all from R&D Systems). For single cell culture, CD150$^+$CD48$^-$KSL HSCs were clonally cultured into 96-well U-bottom plate, and subsequently checked for cell division in each well under a light microscopy after 24 and 48 h. Moreover, to examine an origin of Ca^{2+} influx, 65 µM Nifedipine (Sigma), a Ca^{2+} channel blocker (Shenandoah Biotechnology), or 100 µM 2-Aminoethoxydiphenylborane (2-APB), an inhibitor of IP3 receptor (Sigma), was supplied into the medium.

Quantitative RT-PCR

mRNA expression was assessed using quantitative RT-PCR as described previously (Umemoto et al., 2017).

Analysis for phosphorylated G1-related cell cycle regulators

Intracellular staining was performed using a PerFix EXPOSE kit (Beckman Coulter) according to the manufacturer's instructions. In brief, sorted CD150$^+$CD48$^-$KSL cells were fixed, permeabilized, and staining first with antibodies against CDK4^{pT172} (9H2L7; Thermo Fisher Scientific), CDK6^{pT177} (16HCLC; Thermo Fisher Scientific), and Rb^{pT780} (D20B12; Cell Signaling Technology), and then with a PE-conjugated secondary antibody against rabbit IgG (BioLegend). After staining, the cells were analyzed using flow cytometry.

CFSE dilution assay

Following sorted CD150$^+$CD48$^-$KSL HSCs were stained with 2 µM CFSE (Thermo Fisher Scientific) for 10 min, labeled cells were cultured under indicated conditions. Subsequently, cultured cells with CFSE label were analyzed by a flow cytometer. Highest fluorescent peak in HSCs cultured under undivided conditions (0.5 ng/ml SCF and 0.5 ng/ml TPO) served as undivided cells (zero division).

Promoter motif analysis

After changed genes were extracted from RNA-seq data of both three-divided CD150$^+$CD48$^-$KSL HSCs after the culture in the absence and presence of Nifedipine (more than twofold increase, $P < 0.05$), de novo motif discovery was undertaken on the 500-bp upstream and 100-bp downstream sequences of transcription start sites within Nifedipine–up-regulated genes using DREME (Bailey, 2011), and TOMTOM (Gupta et al., 2007) was used for motif matching.

The measurement of SCF and TPO

After tibias and femurs were flashed out using 500 µl of PBS, cell components were removed from supernatants by the filtration following centrifuge at 300 *g* for 5 min. The amount of SCF or TPO within BM in untreated or 5-FU–treated mice was assessed by using ELISA kit (CUSABIO).

The co-culture with MPs or CD45$^+$ cells

1,000 CD150$^+$CD48$^-$KSL HSCs derived from C57BL/6-Ly5.2 mice were cultured with 30,000 MPs (lineage$^-$c-Kit$^+$Sca-1$^-$) or CD45$^+$ cells obtained from BM of C57BL/6-Ly5.1 mice in S-Clone SF-03 medium supplemented with 0.5% bovine serum albumin, 0.5 ng/ml mouse SCF, and 0.5 ng/ml mouse TPO. After 48 h, the $\Delta\Psi_m$ of HSCs was examined by staining with an antibody for CD45.2 following JC-1 staining. Before the analysis using a flow cytometer, 1 µg/ml propidium iodide (Sigma) was added into cell suspension to assess their viability. To confirm the contribution of adenosine to the suppression of $\Delta\Psi_m$ in HSCs, 10 µM SCH442416 (Sigma), and 10 µM PSB1115 (R&D Systems) were supplied as antagonists for Adora2a and Adora2b, respectively.

The measurement of extracellular adenosine

After tibias and femurs were flashed out using 500 µl of PBS, cell components were removed from supernatants by the filtration following the centrifuge at 300 *g* for 5 min. Adenosine level was determined within obtained supernatants using Adenosine Assay kit according to the manufacturer's instruction (BioVision).

The effect of adenosine on HSCs

To examine the effect of adenosine on $\Delta\Psi_m$ in HSCs in vitro, HSCs were cultured under undivided conditions (0.5 ng/ml SCF and 0.5 ng/ml TPO) with 0.1∼10 µM adenosine (Sigma) for 48 h and subjected to JC-1 staining. To investigate the effect on intracellular Ca^{2+} level, immediately after Fluo-4–labeled HSCs were stimulated with 1 µM adenosine, the fluorescent intensity of Fluo-4 was

Figure 7. **Extracellular adenosine contributes to the maintenance of HSCs during cell divisions after 5-FU administration. (A)** The amount of adenosine within BM in untreated or 5-FU–treated mice (250 mg/kg i.v.; $n = 4$). **(B and C)** The effect of treatment with CV1808 (an agonist of adenosine A2 receptors; 3 mg/kg/shot i.v.) on HSC $\Delta\Psi_m$ (B) or EdC uptake (C). Graphs depict the frequency of JC-1 Red$^+$ cells (B; left), geometric mean fluorescence intensity relative to the value of untreated HSCs (B; right) or EdC$^+$ cells within L$^-$ESLAM HSCs (C). $n = 3$, two independent experiments; *, $P < 0.01$ by *t* test (B); $n = 6$, three independent experiments; **, $P < 0.05$ by *t* test (C). **(D–G)** The effect of the combination between SCH442416 (Adora2a antagonist; 6 mg/kg/shot i.p.) and PSB1115 (Adora2b antagonist; 6 mg/kg/shot i.p.) on HSCs after 5-FU administration. The graph shows $\Delta\Psi_m$ of L$^-$ESLAM cells relative to the value of untreated HSCs (D), total number of nucleated cells (E), or the number of L$^-$ESLAM HSCs (G) within BM. Numbers in dot plots represent the frequency of each fraction within total BM cells (F). Data are presented as means ± SD ($n = 4$, two independent experiments). **(H)** Our proposed model. At steady-state, Ca^{2+}–mitochondria pathway in quiescent HSCs is suppressed through extracellular adenosine provided by surrounding cells (a). 5-FU administration leads to self-renewal division through appropriately loosed adenosine-dependent suppression of Ca^{2+}–mitochondria pathway (b). However, further inhibition of adenosine-mediated suppression attenuates the maintenance of HSCs through more activation of Ca^{2+}–mitochondria pathway (c).

examined by flow cytometry. To examine the role of adenosine A2 receptors in $\Delta\Psi_m$ or intracellular Ca^{2+} level under divided conditions (50 ng/ml SCF and 50 ng/ml TPO), HSCs were treated with 50 µM CV1808 (R&D Systems) for 48 h and subjected to JC-1 or Fluo-4 staining. For in vivo study, 3 mg/kg CV1808 were administrated via i.v. two or three times every 24 h from 1 d after 5-FU treatment, and subsequently $\Delta\Psi_m$ or EdC uptake in HSCs were examined at 3 or 4 d after 5-FU administration, respectively. Moreover, both 6 mg/kg SCH442416 and 6 mg/kg PSB1115 were administrated via i.p. four times every 24 h from 3 d after 5-FU treatment. These treated mice were analyzed at 7 d after 5-FU administration.

Online supplemental material

Fig. S1 shows cell division, mitochondrial statuses and the potential for glucose uptake of HSCs before and after 5-FU administration. Fig. S2 shows the effect of Nifedipine on Ca^{2+} and superoxide level within mitochondria in HSCs. Fig. S3 shows the effect of Isradipine on Ca^{2+}–mitochondria pathway in HSCs. Fig. S4 shows little potential for the suppression of HSC $\Delta\Psi_m$ in mature hematopoietic cells. Fig. S5 shows the effect of CV1808 on Ca^{2+}–mitochondria pathway as well as cell division in HSCs.

Acknowledgments

The authors thank Ms. Miho Kataoka and Ms. Yu Matsuszaki for technical assistances in several experiments.

This study was supported by the National Medical Research Council grant of Singapore Translational Research Investigator Award (NMRC/STaR/0019/2014 to T. Suda), from the Japan Society for the Promotion of Science (JSPS) Grant-in-Aid for Young Scientists (17K16190; to T. Umemoto) and Grant-in-Aid for Scientific Research (26221309 to T. Suda), the Ichiro Kanehara Foundation (to T. Umemoto), Friends of Leukemia Research Fund (to T. Umemoto), and the Shinnihon Foundation of Advanced Medical Treatment Research (to T. Umemoto).

The authors declare no competing financial interests.

Author contributions: T. Umemoto and T. Suda designed the study and wrote the manuscript. T. Umemoto performed most of the experiments. M. Hashimoto and A. Nakamura-Ishizu helped with several experiments. A. Nakamura-Ishizu edited the manuscript. T. Mastumura performed promoter motif analysis.

Submitted: 5 March 2018
Revised: 14 May 2018
Accepted: 11 June 2018

References

Akada, H., S. Akada, R.E. Hutchison, K. Sakamoto, K.U. Wagner, and G. Mohi. 2014. Critical role of Jak2 in the maintenance and function of adult hematopoietic stem cells. Stem Cells. 32:1878–1889. https://doi.org/10.1002/stem.1711

Bailey, T.L. 2011. DREME: motif discovery in transcription factor ChIP-seq data. Bioinformatics. 27:1653–1659. https://doi.org/10.1093/bioinformatics/btr261

Baldridge, M.T., K.Y. King, N.C. Boles, D.C. Weksberg, and M.A. Goodell. 2010. Quiescent haematopoietic stem cells are activated by IFN-gamma in response to chronic infection. Nature. 465:793–797. https://doi.org/10.1038/nature09135

Bidaux, G., A.S. Borowiec, D. Gordienko, B. Beck, G.G. Shapovalov, L. Lemonnier, M. Flourakis, M. Vandenberghe, C. Slomianny, E. Dewailly, et al. 2015. Epidermal TRPM8 channel isoform controls the balance between keratinocyte proliferation and differentiation in a cold-dependent manner. Proc. Natl. Acad. Sci. USA. 112:E3345–E3354. https://doi.org/10.1073/pnas.1423357112

Chen, J.Y., M. Miyanishi, S.K. Wang, S. Yamazaki, R. Sinha, K.S. Kao, J. Seita, D. Sahoo, H. Nakauchi, and I.L. Weissman. 2016. Hoxb5 marks long-term haematopoietic stem cells and reveals a homogenous perivascular niche. Nature. 530:223–227. https://doi.org/10.1038/nature16943

Cheng, T., N. Rodrigues, H. Shen, Y. Yang, D. Dombkowski, M. Sykes, and D.T. Scadden. 2000. Hematopoietic stem cell quiescence maintained by p21cip1/waf1. Science. 287:1804–1808. https://doi.org/10.1126/science.287.5459.1804

Cho, J., R. Yusuf, S. Kook, E. Attar, D. Lee, B. Park, T. Cheng, D.T. Scadden, and B.C. Lee. 2014. Purinergic $P2Y_{14}$ receptor modulates stress-induced hematopoietic stem/progenitor cell senescence. J. Clin. Invest. 124:3159–3171. https://doi.org/10.1172/JCI61636

Essers, M.A., S. Offner, W.E. Blanco-Bose, Z. Waibler, U. Kalinke, M.A. Duchosal, and A. Trumpp. 2009. IFNalpha activates dormant haematopoietic stem cells in vivo. Nature. 458:904–908. https://doi.org/10.1038/nature07815

Fukumori, R., T. Takarada, R. Nakazato, K. Fujikawa, M. Kou, E. Hinoi, and Y. Yoneda. 2013. Selective inhibition by ethanol of mitochondrial calcium influx mediated by uncoupling protein-2 in relation to N-methyl-D-aspartate cytotoxicity in cultured neurons. PLoS One. 8:e69718. https://doi.org/10.1371/journal.pone.0069718

Gazit, R., P.K. Mandal, W. Ebina, A. Ben-Zvi, C. Nombela-Arrieta, L.E. Silberstein, and D.J. Rossi. 2014. Fgd5 identifies hematopoietic stem cells in the murine bone marrow. J. Exp. Med. 211:1315–1331. https://doi.org/10.1084/jem.20130428

Gupta, S., J.A. Stamatoyannopoulos, T.L. Bailey, and W.S. Noble. 2007. Quantifying similarity between motifs. Genome Biol. 8:R24. https://doi.org/10.1186/gb-2007-8-2-r24

Hajnóczky, G., L.D. Robb-Gaspers, M.B. Seitz, and A.P. Thomas. 1995. Decoding of cytosolic calcium oscillations in the mitochondria. Cell. 82:415–424. https://doi.org/10.1016/0092-8674(95)90430-1

Ham, J., and B.A. Evans. 2012. An emerging role for adenosine and its receptors in bone homeostasis. Front. Endocrinol. (Lausanne). 3:113.

Harrison, D.E., and C.P. Lerner. 1991. Most primitive hematopoietic stem cells are stimulated to cycle rapidly after treatment with 5-fluorouracil. Blood. 78:1237–1240.

Hawkins, B.J., K.M. Irrinki, K. Mallilankaraman, Y.C. Lien, Y. Wang, C.D. Bhanumathy, R. Subbiah, M.F. Ritchie, J. Soboloff, Y. Baba, et al. 2010. S-glutathionylation activates STIM1 and alters mitochondrial homeostasis. J. Cell Biol. 190:391–405. https://doi.org/10.1083/jcb.201004152

Hayashi, T., H. Ozaki, Y. Sasagawa, M. Umeda, H. Danno, and I. Nikaido. 2018. Single-cell full-length total RNA sequencing uncovers dynamics of recursive splicing and enhancer RNAs. Nat. Commun. 9:619. https://doi.org/10.1038/s41467-018-02866-0

Hills, D., R. Gribi, J. Ure, N. Buza-Vidas, S. Luc, S.E. Jacobsen, and A. Medvinsky. 2011. Hoxb4-YFP reporter mouse model: a novel tool for tracking HSC development and studying the role of Hoxb4 in hematopoiesis. Blood. 117:3521–3528. https://doi.org/10.1182/blood-2009-12-253989

Hirata, Y., K. Furuhashi, H. Ishii, H.W. Li, S. Pinho, L. Ding, S.C. Robson, P.S. Frenette, and J. Fujisaki. 2018. $CD150^{high}$ Bone Marrow Tregs Maintain Hematopoietic Stem Cell Quiescence and Immune Privilege via Adenosine. Cell Stem Cell. 22:445–453.e5. https://doi.org/10.1016/j.stem.2018.01.017

Ito, K., and T. Suda. 2014. Metabolic requirements for the maintenance of self-renewing stem cells. Nat. Rev. Mol. Cell Biol. 15:243–256. https://doi.org/10.1038/nrm3772

Iwasaki, H., C. Somoza, H. Shigematsu, E.A. Duprez, J. Iwasaki-Arai, S. Mizuno, Y. Arinobu, K. Geary, P. Zhang, T. Dayaram, et al. 2005. Distinctive and indispensable roles of PU.1 in maintenance of hematopoietic stem cells and their differentiation. Blood. 106:1590–1600. https://doi.org/10.1182/blood-2005-03-0860

Jiang, L.H., F. Mousawi, X. Yang, and S. Roger. 2017. ATP-induced Ca^{2+}-signalling mechanisms in the regulation of mesenchymal stem cell migration. Cell. Mol. Life Sci. 74:3697–3710. https://doi.org/10.1007/s00018-017-2545-6

Jouaville, L.S., P. Pinton, C. Bastianutto, G.A. Rutter, and R. Rizzuto. 1999. Regulation of mitochondrial ATP synthesis by calcium: evidence for

a long-term metabolic priming. Proc. Natl. Acad. Sci. USA. 96:13807–13812. https://doi.org/10.1073/pnas.96.24.13807

Kataoka, K., T. Sato, A. Yoshimi, S. Goyama, T. Tsuruta, H. Kobayashi, M. Shimabe, S. Arai, M. Nakagawa, Y. Imai, et al. 2011. Evi1 is essential for hematopoietic stem cell self-renewal, and its expression marks hematopoietic cells with long-term multilineage repopulating activity. J. Exp. Med. 208:2403–2416. https://doi.org/10.1084/jem.20110447

Kent, D.G., M.R. Copley, C. Benz, S. Wöhrer, B.J. Dykstra, E. Ma, J. Cheyne, Y. Zhao, M.B. Bowie, Y. Zhao, et al. 2009. Prospective isolation and molecular characterization of hematopoietic stem cells with durable self-renewal potential. Blood. 113:6342–6350. https://doi.org/10.1182/blood-2008-12-192054

Kirichok, Y., G. Krapivinsky, and D.E. Clapham. 2004. The mitochondrial calcium uniporter is a highly selective ion channel. Nature. 427:360–364. https://doi.org/10.1038/nature02246

Kubota, Y., M. Osawa, L.M. Jakt, K. Yoshikawa, and S. Nishikawa. 2009. Necdin restricts proliferation of hematopoietic stem cells during hematopoietic regeneration. Blood. 114:4383–4392. https://doi.org/10.1182/blood-2009-07-230292

Liu, Y., S.E. Elf, Y. Miyata, G. Sashida, Y. Liu, G. Huang, S. Di Giandomenico, J.M. Lee, A. Deblasio, S. Menendez, et al. 2009. p53 regulates hematopoietic stem cell quiescence. Cell Stem Cell. 4:37–48. https://doi.org/10.1016/j.stem.2008.11.006

Mantel, C.R., H.A. O'Leary, B.R. Chitteti, X. Huang, S. Cooper, G. Hangoc, N. Brustovetsky, E.F. Srour, M.R. Lee, S. Messina-Graham, et al. 2015. Enhancing Hematopoietic Stem Cell Transplantation Efficacy by Mitigating Oxygen Shock. Cell. 161:1553–1565. https://doi.org/10.1016/j.cell.2015.04.054

Mendelson, A., and P.S. Frenette. 2014. Hematopoietic stem cell niche maintenance during homeostasis and regeneration. Nat. Med. 20:833–846. https://doi.org/10.1038/nm.3647

Min, I.M., G. Pietramaggiori, F.S. Kim, E. Passegué, K.E. Stevenson, and A.J. Wagers. 2008. The transcription factor EGR1 controls both the proliferation and localization of hematopoietic stem cells. Cell Stem Cell. 2:380–391. https://doi.org/10.1016/j.stem.2008.01.015

Miyamoto, K., K.Y. Araki, K. Naka, F. Arai, K. Takubo, S. Yamazaki, S. Matsuoka, T. Miyamoto, K. Ito, M. Ohmura, et al. 2007. Foxo3a is essential for maintenance of the hematopoietic stem cell pool. Cell Stem Cell. 1:101–112. https://doi.org/10.1016/j.stem.2007.02.001

Pietras, E.M., R. Lakshminarasimhan, J.M. Techner, S. Fong, J. Flach, M. Binnewies, and E. Passegué. 2014. Re-entry into quiescence protects hematopoietic stem cells from the killing effect of chronic exposure to type I interferons. J. Exp. Med. 211:245–262. https://doi.org/10.1084/jem.20131043

Ralevic, V., and G. Burnstock. 1998. Receptors for purines and pyrimidines. Pharmacol. Rev. 50:413–492.

Renault, V.M., P.U. Thekkat, K.L. Hoang, J.L. White, C.A. Brady, D. Kenzelmann Broz, O.S. Venturelli, T.M. Johnson, P.R. Oskoui, Z. Xuan, et al. 2011. The pro-longevity gene FoxO3 is a direct target of the p53 tumor suppressor. Oncogene. 30:3207–3221. https://doi.org/10.1038/onc.2011.35

Sawai, C.M., S. Babovic, S. Upadhaya, D.J.H.F. Knapp, Y. Lavin, C.M. Lau, A. Goloborodko, J. Feng, J. Fujisaki, L. Ding, et al. 2016. Hematopoietic Stem Cells Are the Major Source of Multilineage Hematopoiesis in Adult Animals. Immunity. 45:597–609. https://doi.org/10.1016/j.immuni.2016.08.007

Stella, S.L. Jr., E.J. Bryson, and W.B. Thoreson. 2002. A2 adenosine receptors inhibit calcium influx through L-type calcium channels in rod photoreceptors of the salamander retina. J. Neurophysiol. 87:351–360. https://doi.org/10.1152/jn.00010.2001

Subramanian, A., P. Tamayo, V.K. Mootha, S. Mukherjee, B.L. Ebert, M.A. Gillette, A. Paulovich, S.L. Pomeroy, T.R. Golub, E.S. Lander, and J.P. Mesirov. 2005. Gene set enrichment analysis: a knowledge-based approach for interpreting genome-wide expression profiles. Proc. Natl. Acad. Sci. USA. 102:15545–15550. https://doi.org/10.1073/pnas.0506580102

Suda, T., K. Takubo, and G.L. Semenza. 2011. Metabolic regulation of hematopoietic stem cells in the hypoxic niche. Cell Stem Cell. 9:298–310. https://doi.org/10.1016/j.stem.2011.09.010

Svenningsson, P., C. Le Moine, G. Fisone, and B.B. Fredholm. 1999. Distribution, biochemistry and function of striatal adenosine A2A receptors. Prog. Neurobiol. 59:355–396. https://doi.org/10.1016/S0301-0082(99)00011-8

Takubo, K., N. Goda, W. Yamada, H. Iriuchishima, E. Ikeda, Y. Kubota, H. Shima, R.S. Johnson, A. Hirao, M. Suematsu, and T. Suda. 2010. Regulation of the HIF-1alpha level is essential for hematopoietic stem cells. Cell Stem Cell. 7:391–402. https://doi.org/10.1016/j.stem.2010.06.020

Tarasov, A.I., F. Semplici, M.A. Ravier, E.A. Bellomo, T.J. Pullen, P. Gilon, I. Sekler, R. Rizzuto, and G.A. Rutter. 2012. The mitochondrial Ca2+ uniporter MCU is essential for glucose-induced ATP increases in pancreatic β-cells. PLoS One. 7:e39722. https://doi.org/10.1371/journal.pone.0039722

Umemoto, T., M. Yamato, Y. Shiratsuchi, M. Terasawa, J. Yang, K. Nishida, Y. Kobayashi, and T. Okano. 2006. Expression of Integrin beta3 is correlated to the properties of quiescent hemopoietic stem cells possessing the side population phenotype. J. Immunol. 177:7733–7739. https://doi.org/10.4049/jimmunol.177.11.7733

Umemoto, T., M. Yamato, J. Ishihara, Y. Shiratsuchi, M. Utsumi, Y. Morita, H. Tsukui, M. Terasawa, T. Shibata, K. Nishida, et al. 2012. Integrin-αvβ3 regulates thrombopoietin-mediated maintenance of hematopoietic stem cells. Blood. 119:83–94. https://doi.org/10.1182/blood-2011-02-335430

Umemoto, T., Y. Matsuzaki, Y. Shiratsuchi, M. Hashimoto, T. Yoshimoto, A. Nakamura-Ishizu, B. Petrich, M. Yamato, and T. Suda. 2017. Integrin αvβ3 enhances the suppressive effect of interferon-γ on hematopoietic stem cells. EMBO J. 36:2390–2403. https://doi.org/10.15252/embj.201796771

Vannini, N., M. Girotra, O. Naveiras, G. Nikitin, V. Campos, S. Giger, A. Roch, J. Auwerx, and M.P. Lutolf. 2016. Specification of haematopoietic stem cell fate via modulation of mitochondrial activity. Nat. Commun. 7:13125. https://doi.org/10.1038/ncomms13125

Zeng, H., R. Yücel, C. Kosan, L. Klein-Hitpass, and T. Möröy. 2004. Transcription factor Gfi1 regulates self-renewal and engraftment of hematopoietic stem cells. EMBO J. 23:4116–4125. https://doi.org/10.1038/sj.emboj.7600419

Zhang, C.C., and H.F. Lodish. 2005. Murine hematopoietic stem cells change their surface phenotype during ex vivo expansion. Blood. 105:4314–4320. https://doi.org/10.1182/blood-2004-11-4418